The RNS/Prandtl equations and their link with other asymptotic descriptions

P.-Y. Lagrée
CNRS & UPMC Univ Paris 06, UMR 7190,
Institut Jean Le Rond dAlembert, Boîte 162, F-75005 Paris, France
pyl@ccr.jussieu.fr ; www.lmm.jussieu.fr/∼lagree

September 8, 2009

Abstract

In this chapter, a steady laminar axisymmetrical flow in a straight constricted pipe is considered (then the same 2D problem between two parallel plates is considered). The RNS/Prandtl equations are presented as an asymptotic limit of the Navier-Stokes equations. This set of equations is shown to include at first order several asymptotic descriptions of the full Navier-Stokes equations: the Blasius régime, Interacting Boundary Layer theory, Triple Deck theory, the Poiseuille régime and Double Deck theory. These theories are all characterised by a constant pressure in each cross section. Thus, these equations are able to describe the transitions between flow regions that correspond to different classical asymptotic descriptions or regimes that are usually done with the full Navier-Stokes Equations. Some prediction on the magnitude of the wall shear stress and on the pressure drop will be compared with Navier-Stokes computations for cases of severe constrictions.

This text is in fact very similar to the three papers "The RNS/Prandtl equations and their link with other asymptotic descriptions: application to the wall shear stress scaling in a constricted pipe" by P.-Y. Lagrée & Sylvie Lorthois in International Journal of Engineering Sciences (2005), [22], and to "Characterization of the pressure drop in a 2D symmetrical pipe: some asymptotical, numerical and experimental comparisons" by P.-Y. Lagre, E. Berger, M. Deverge, C. Vilain & A. Hirschberg (2005): Z. Angew. Math. Mech. [18], and to "Asymmetrical effects in a 2D stenosis" by P.-Y. Lagre, A. Van Hirtum & X. Pelorson (2007): European Journal of Mechanics - B/Fluids, [19].

1 Introduction

Estimating the flow quantities like the magnitude of the wall shear stress (WSS) or the pressure drop in a locally constricted pipe is important in numerous applications. For example, elevated wall shear stresses encountered in stenoses, *i.e.* local constrictions of blood vessels, play a significant role in thrombo-embolism and atherosclerotic plaques ruptures (Berger and Jou [1], Stroud et al. [47]). Of course, computing the flow in such a pipe can be achieved with great accuracy through Navier-Stokes solvers (Budwig et al. [2], Bluestein et al. [3] de Bruin et al. [8], Siegel et al. [40]). However, asymptotic equations provides a better understanding of the flow structure and relevant scalings, and reduces computational time. Therefore, parameters may be changed easily and their influence can be thoroughly investigated. Hence, the aim of this work is to find the appropriate scaling for the wall shear stress in a constricted pipe as a function of pertinent non-dimensional parameters using an asymptotic approach.
For that purpose, a set of equations that is sometimes referred to as Reduced Navier-Stokes (RNS) equations will be our starting point. These equations, including a transverse pressure gradient, can be found either in three or two dimensions, plane or axisymmetrical, in Fletcher [10] and Tannehil *et al.* [49]. However, in our analysis, these equations will be used with a constant transverse pressure, *i.e.* the pressure is a function of x alone : $\partial_r p = 0$ or $p(x)$. In this case, the RNS equations formally correspond to the Prandtl equations, but with different boundary conditions. Therefore, they may be called RNS/Prandtl, or RNSP(x).
Following Smith [41] and other authors (e. g. Saintlos & Mauss [37], Sychev et al. [48]) analyses, we will show that the RNS/Prandtl equations includes many classical asymptotic descriptions for internal flows, *i.e.* the Interactive Boundary Layer (IBL), the Double Deck and the Triple Deck theories, as well as Blasius and Poiseuille regimes. Thus, the RNS/Prandtl equations are able to describe the transitions between flow regions that correspond to different classical asymptotic descriptions or regimes that are usually done with the full Navier-Stokes Equations.
In order to demonstrate the "universality" of the RNSP(x) equations, we will use either the least possible degeneracy principle (Van Dyke [50]), which requires the inertia-pressure-viscous force balance, or directly the results from the literature, that are classical but till have been disjoined.
The limitation of this description will also be presented. In particular, the RNSP(x) equations are not valid when $\partial_r p$ is not zero, which induces ellipticity and prevents the flow from being solved with a streamwise marching

procedure. Nevertheless, this is not a very strong condition in internal flows, and will be demonstrated using the Double Deck and Triple Deck theories. In particular, calculation of separated flows is possible (Smith [41], Sychev et all. [48], Lagrée et al. [21]). Hence, the RNSP(x) equations may be applied in the case of a dilated pipe or aneurysm (Lagrée [16], Budwig et al. [2] and Bluestein et al. [3]). In addition, the RNSP(x) formulation can be applied to supersonic external flows (see Davis et al. [7]) except when there is an upstream influence from the flow downstream, which occurs in some Triple Deck problems (Stewartson [45]). A case of a hypersonic external flow has also been studied by Maslov et al. [26] by a RNS computation without obtaining branching solutions from upstream influence.
In the following, the variables with stars denote dimensional variables.

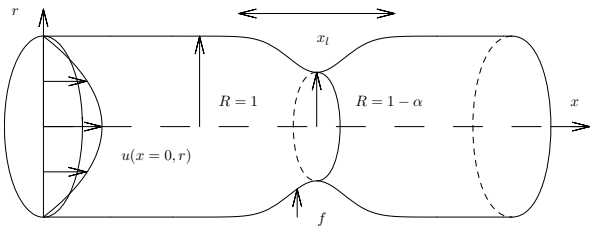

Figure 1: **Geometrical parameters of the constricted pipe.** Note that the transverse scale is non-dimensionalised by the unperturbed pipe radius R_0^*. Values of x_l and α are linked *via* the asymptotic scales.

Part I
Axi case

2 RNS/Prandtl equations (RNSP(x))

2.1 The RNSP(x) hypothesis

We consider a steady laminar incompressible axisymmetrical flow of a Newtonian fluid in a locally constricted axisymmetric pipe (see Fig. 1 for notations used). The radial position of the pipe is given by : $R^* = R_0^*(1-f(x^*))$, where R_0^* is the unconstricted radius and f is the given radius perturbation. In addition, we denote by U_0^* the longitudinal velocity scale of the flow and assume that the typical length scale for transverse variations of the longitudinal velocity is R_0^*. From the Navier-Stokes equations, we obtain a longitudinal scale ($L_{RNS}^* >> R_0^*$) from a balance between the convective term and the largest diffusive term. In other words, $(u^* \frac{\partial u^*}{\partial x^*})$ must be of the same order as $\nu \frac{\partial}{r^* \partial r^*}(r^* \frac{\partial}{\partial r^*} u^*)$, which leads to:

$$\frac{U_0^{*2}}{L_{RNS}^*} u \frac{\partial u}{\partial x} \simeq \nu \frac{U_0^*}{R_0^{*2}} \frac{\partial}{r \partial r}(r \frac{\partial}{\partial r} u), \tag{1}$$

where ν is the kinematic viscosity. Thus the longitudinal scale L_{RNS}^* equals $R_0^* Re$, where Re is the Reynolds number $Re = U_0^* R_0^* / \nu$. Finally, the pressure and transverse velocity scales are determined from a balance among the viscous term, convective term, and pressure gradient that drives the flow (Van Dyke [50]). Of course, this is similar to the classical way to obtain the Prandtl equations although in the Prandtl case the transversal scale is deduced from an initially chosen longitudinal scale.
A similar approach will be carried out in the following sections with various transverse scales corresponding to the tickness of additional layers near the wall, and with various scales for the longitudinal velocity in these new layers. A longitudinal length scale will still be determined in order to obtain a balance among inertia, pressure, viscous forces.

2.2 The RNSP(x) Formulation

As deduced from the previous section, the non-dimensional variables are given by :
$x^* = x R_0^* Re$, $r^* = r R_0^*$, $u^* = U_0^* u$, $v^* = \frac{U_0^*}{Re} v$, $p^* = p_0^* + \rho_0 U_0^{*2} p$,

p_0^* denoting the entry pressure, and, consequently :

$$\tau^* = \mu \frac{\partial u^*}{\partial r^*} = \frac{\rho U_0^{*2}}{Re} \tau, \tag{2}$$

where τ is the WSS, μ is the dynamic viscosity and ρ the density.
With these new variables, the following partial differential system is obtained from the Navier-Stokes equations as $Re \to \infty$:

$$\frac{\partial}{\partial x} u + \frac{\partial rv}{r \partial r} = 0, \qquad u \frac{\partial u}{\partial x} + v \frac{\partial u}{\partial r} = -\frac{\partial p}{\partial x} + \frac{\partial}{r \partial r}(r \frac{\partial u}{\partial r}), \qquad 0 = -\frac{\partial p}{\partial r}. \tag{3}$$

The associated boundary conditions are:

- the condition of axial symmetry : $\partial_r u = 0$ and $v = 0$ at $r = 0$,
- no-slip condition at the wall : $u = v = 0$ at $r = 1 - f(x)$. Of course, in order to apply the RNSP(x) set, f is of order one, but smaller than one, and the longitudinal scale has to be compatible, *i.e.* of scale L^*_{RNS}. In the next section, the implications of a change in the constriction height and the length will be discussed,
- the entry velocity profiles ($u(0, r)$ and $v(0, r)$) are given : flat profile or Poiseuille flow, but other profile is also possible,
- there is *no* outflow boundary condition because the system is parabolic as will be demonstrated in the linearised asymptotic descriptions. The equations are solved by marching in the streamwise direction, even if there is flow separation.

The most important result of the computation is the non-dimensionalised WSS: $\tau = \frac{\partial u}{\partial r}(x, 0)$.

2.3 Comments

This set of equations has been already used for studying entry effects by Cebeci & Cousteix [4] and in Schlichting [38]. However, Rubin & Himansu [36] and Tannehil et al. [10] kept a transversal pressure variation linked with the transverse velocity as follows:

$$Re^{-2}(u \frac{\partial}{\partial x} v + v \frac{\partial}{\partial r} v) = -\frac{\partial p}{\partial r} + Re^{-2}(\frac{\partial}{r \partial r}(r \frac{\partial}{\partial r} v) - \frac{v^2}{r}). \tag{4}$$

They call the system (3.1 , 3.2, 4) "Reduced NS", but as noted by Fletcher [10], this system contains a mix of orders of magnitude, and is not coherent

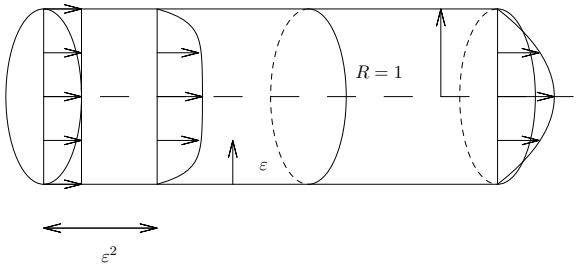

Figure 2: **Unconstricted situation : entry problem.** Starting from a flat velocity profile, a Poiseuille profile is obtained at the exit, *i.e.* at a distance $O(1)$ in the $R_0 Re$ scale. Near the entrance, *i.e.* at a distance $O(\varepsilon^2)$, the IBL formulation is valid : the boundary layer thickness is of order $O(\varepsilon)$ in the R_0 scale.

from an asymptotical point of view. Indeed, as Re tends toward infinity, Eq. 4 degenerates to Eq. 3.3, and the system (3.1, 3.2, 4) reduces to the RNSP(x) set. Subsequently, this system is used to obtain most of the degeneracy of the full NS equations in an axisymmetrical pipe :

- In §3.1, a unconstricted case will be discussed (entry problem, see Fig. 2),
- In §3.2.1 and §3.3, a case of a constriction situated near the pipe entry, where the velocity profile is flat in the core flow, will be considered (see Fig. 3, left). In this case, the Interacting Boundary Layer and the Triple Deck theories are valid since the core flow is inviscid and there is a thin boundary layer near the wall,
- In §3.4, a case of a constriction situated far from the pipe entry, where the flow is fully developed, will be considered (see Fig. 3, right). In this region, the Double Deck theory, also known as Smith's theory of viscous perturbation on a Poiseuille flow in a pipe, is valid,
- Finally, in §3.6.1, we will show that if the constriction is short compared to $R_0^* Re$, the velocity profile at the entry is not important. In that case, the Interacting Boundary Layer theory proves to be valid again: acceleration is so high that the profile flattens, recreating an inviscid core and a thin boundary layer near the wall.

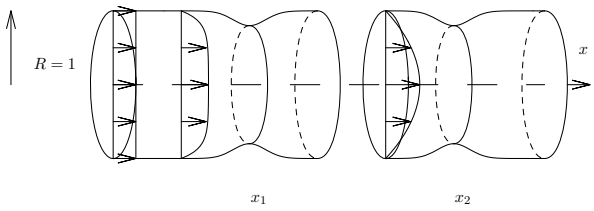

Figure 3: **Flow configurations :** A constriction may be located at station x_1 where an inviscid fluid core still exists, see §3.2.1: IBL or §3.3: Triple Deck (Fig. 8), or at station x_2 where the Poiseuille profile has developed, see §3.4: Double Deck (Fig. 11). If the constriction is short but severe enough, the exact entrance velocity profile has no importance, see §3.6.1: IBL.

In particular, the scale of the non-dimensional WSS will be determined by the location and size of the constriction. This scale will not always be of order one in the RNSP scales.

3 Link of RNSP(x) with other Asymptotic descriptions.

3.1 RNSP(x): from Blasius to Poiseuille

First, starting from a flat profile at the entrance ($u(0,r)=1$ and $v(0,r)=0$), the flow consist of two concentric layers (see Fig. 2) :

- A first layer of length $\varepsilon^2 << 1$ and of transversal length 1 (except near the wall) where the velocity is uniform ($u=1$, $v=0$): the inviscid core,

- A second thin layer of the same longitudinal length $\varepsilon^2 << 1$, but of thickness $\varepsilon << 1$. In this layer, introducing $x=\varepsilon^2\bar{x}$, $r=1-\varepsilon\bar{y}$, $u=\bar{u}$, $-v=\varepsilon^{-1}\bar{v}$ and $p=\bar{p}$, the RNSP(x) set leads to the classical Boundary Layer equations:

$$\frac{\partial\bar{u}}{\partial\bar{x}}+\frac{\partial\bar{v}}{\partial\bar{y}}=0, \qquad (\bar{u}\frac{\partial\bar{u}}{\partial\bar{x}}+\bar{v}\frac{\partial\bar{u}}{\partial\bar{y}})=-\frac{\partial\bar{p}}{\partial\bar{x}}+\frac{\partial^2\bar{u}}{\partial\bar{y}^2}, \qquad 0=-\frac{\partial\bar{p}}{\partial\bar{y}}, \quad (5)$$

  with the following boundary conditions : $\bar{u}(\bar{x},0)=0$, $\bar{v}(\bar{x},0)=0$, $\bar{u}(\bar{x},\infty)=1$, $\bar{p}(\bar{x},\infty)=0$, corresponding to the Blasius flow regime.

  Thus, if L^* denotes the current dimensional length in this second layer, *i.e.* $L^*=\varepsilon^2 L^*_{RNS}$, the corresponding thickness is given by εR^*_0, or :

$$\sqrt{\frac{L^*}{L^*_{RNS}}}R^*_0=\frac{L^*}{\sqrt{\frac{U^*_0 L^*}{\nu}}}, \quad (6)$$

  the classical boundary layer thickness. Similarly, the non-dimensional WSS is the Blasius value $\bar{\tau}=0.33\bar{x}^{-1/2}$ (Schlichting [38]). Consequently, $\tau=\varepsilon^{-1}0.33(\varepsilon^{-2}x)^{-1/2}$, or, in dimensional form :

$$\tau^*=[\frac{\rho U^{*2}_0}{Re}](0.33(\frac{x^*}{R^*_0})^{-1/2}). \quad (7)$$

Second, the Poiseuille solution is obviously a solution for the set (3) associated with the no-slip condition at the wall , with its WSS:

$$u=U_{Pois}(r)=2(1-r^2), \qquad v=0, \qquad \tau^*=(4)[\frac{\rho U^{*2}_0}{Re}]. \quad (8)$$

Third, the system (3) allows the computation of the entry flow from Blasius to Poiseuille (see Schlichting [38], Cebeci & Cousteix [4] and next subsection).
Finally, at the entrance of the pipe, there is a small region of the same relative thickness and length $\varepsilon = Re^{-1}$ where a full Navier-Stokes problem must be solved. This degeneracy is not included in the RNSP(x). From Navier-Stokes equations, with: $x^* = \varepsilon R_0^* \hat{x}$, $r^* = R_0^*(1 - \varepsilon\hat{y})$, $u^* = U_0^* \hat{u}$, $v^* = U_0^* \hat{v}$ we obtain:

$$\frac{\partial \hat{u}}{\partial \hat{x}} + \frac{\partial \hat{v}}{\partial \hat{y}} = 0 \tag{9}$$

$$\hat{u}\frac{\partial \hat{u}}{\partial \hat{x}} + \hat{v}\frac{\partial \hat{u}}{\partial \hat{y}} = -\frac{\partial \hat{p}}{\partial \hat{x}} + \frac{\partial^2 \hat{u}}{\partial \hat{x}^2} + \frac{\partial^2 \hat{u}}{\partial \hat{y}^2}, \quad \hat{u}\frac{\partial \hat{v}}{\partial \hat{x}} + \hat{v}\frac{\partial \hat{v}}{\partial \hat{y}} = -\frac{\partial \hat{p}}{\partial \hat{y}} + \frac{\partial^2 \hat{v}}{\partial \hat{x}^2} + \frac{\partial^2 \hat{v}}{\partial \hat{y}^2} \tag{10}$$

This short scale problem is the first limitation of the RNSP(x) set because $\partial\hat{p}/\partial\hat{y}$ is not zero, resulting an elliptic system. In this region, in the RNSP scales, the transversal length is of order Re^{-1} and the longitudinal velocity is of order 1. The non-dimensional WSS thus scales as Re. Finally, from Eq. 2, the physical scale of the WSS (τ^*) is given by

$$\tau^* = O(\rho U_0^{*2}). \tag{11}$$

Note that the matching between this NS short scale region and the RNS/Prandtl areas is a very difficult task. However, there is an analogy between this issue and the thermal boundary layer in a Poiseuille flow (described in Pedley [30]). First, at the entrance of the pipe, the full heat equation holds, corresponding to our full NS problem. Then, the Lévêque problem corresponds to our inviscid core/Blasius layer flow region. Finally, the Graetz problem corresponds to the Blasius/Poiseuille transition. In this problem, solutions of the full heat equations may be matched with the solution of the Lévêque problem.

3.1.1 Numerical results

The numerical solutions of the RNSP system (3.1, 3.2, 3.3) and other asymptotic descriptions in the following sections are achieved using a simple finite difference scheme in "mapped variables" (Lagrée [17]). The derivatives are implicit, centered in the transverse direction and marching in the streamwise direction. The core of the solution is the second order derivative with a two point boundary condition for u in Eq. 3.2. It is solved by the Thomas algorithm (Peyret & Taylor [32]). The transverse velocity is then computed by integration of Eq. 3. The idea is to guess by a Newton iteration scheme

the value of the pressure at the current step so that the boundary condition for the transverse velocity is fulfilled. An alternative way to solve for the pressure gradient can be found in Feltcher [10]. This code enables the computation of the boundary layer separation (reverse flow) in mild constrictions, but, if the constriction is severe, the FLARE approximation (Reyhner & Flügge Lotz [33]) must be used .
Fig. 4 displays the longitudinal evolution of the velocity at the centre of the pipe, starting from the entrance ($u(x = 0, r = 0) = 1$) and to the Poiseuille value ($u(x = \infty, r = 0) = 2$)). The length of the entrance region is given by $x_e \simeq 0.214$ where $u(x_e, r = 0)/u(x = \infty, r = 0)$ equals 0.99. The asymptote obtained for small $x = 0$ values will be examined in the next section. Fig. 5 displays the longitudinal evolution of the pressure. For large x, the pressure asymptote is linear and of slope -8 as expected from Eqs. 5 and 8. The intercept of this asymptote corresponds to the singular pressure drop Δp_{entry} for an entry flow, *i.e.* : $\Delta p_{entry} = -0.63$.

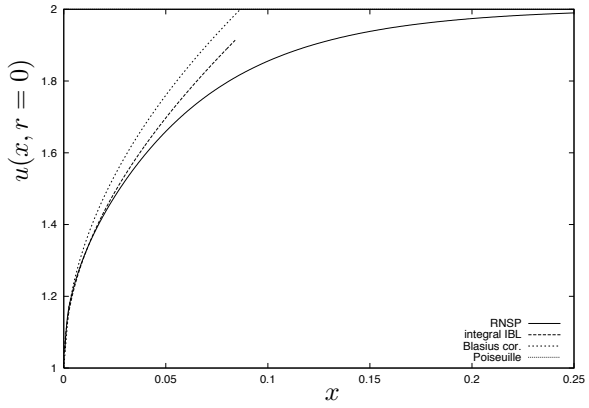

Figure 4: **Unconstricted situation : longitudinal evolution of the velocity at the centre of the pipe.** RNSP : numerical solution of the RNSP equations ; integral IBL : solution obtained with the integral IBL approach, rescaled in the x variable ; "Blasius cor." : first order correction ($u = 1 + 3.4x^{1/2}$) to the Blasius solution (which is $u = 1$), as obtained in §3.2.5. Note that the Poiseuille value is independent of x and equals 2.

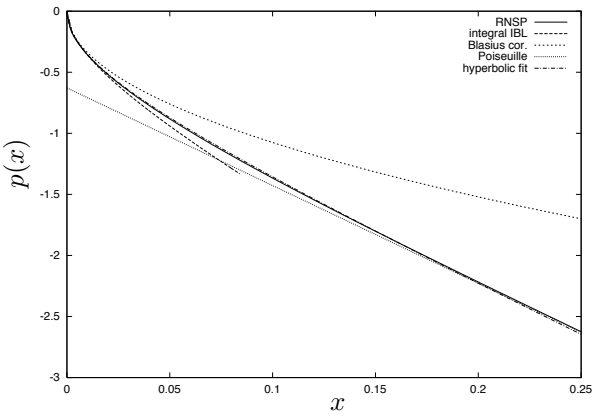

Figure 5: **Unconstricted situation : longitudinal evolution of the pressure :** RNSP : numerical solution of the RNSP equations ; integral IBL : solution obtained with the integral IBL approach, rescaled in the x variable ; Poiseuille : $p = -0.63 - 8x$, see §3.1 ; Blasius cor. : first order correction ($-2\varepsilon\bar{\delta}_{1Blasius}$) to the Blasius solution (which is $p = 0$), as obtained in §3.2.5 ; hyperbolic fit : *ad hoc* fitting relation (Eq. 20).

3.2 RNSP(x): the link with IBL (Interacting Boundary Layer)

3.2.1 The IBL Formulation

After rescaling: $r = 1 - \varepsilon\bar{y}$, $u = \bar{u}$, $v = -\varepsilon^{-1}\bar{v}$, $x = \varepsilon^2\bar{x}$ and $p = \bar{p}$ and assuming a flat entry velocity profile, the RNSP(x) leads to the final IBL formulation as follows:

$$\frac{\partial\bar{u}}{\partial\bar{x}} + \frac{\partial\bar{v}}{\partial\bar{y}} = 0, (\bar{u}\frac{\partial\bar{u}}{\partial\bar{x}} + \bar{v}\frac{\partial\bar{u}}{\partial\bar{y}}) = \bar{u}_e\frac{d\bar{u}_e}{d\bar{x}} + \frac{\partial^2\bar{u}}{\partial\bar{y}^2}, \tag{12}$$

$$\bar{u}_e = \frac{1}{(1 - 2\varepsilon\bar{\delta}_1)} \tag{13}$$

where $\bar{\delta}_1 = \int_0^\infty (1 - \frac{\bar{u}}{\bar{u}_e})d\bar{y}$ and with the following boundary conditions :
$\bar{u}(\bar{x}, 0) = 0$, $\bar{v}(\bar{x}, 0) = 0$ and $\bar{u}(\bar{x}, \infty) = \bar{u}_e$

3.2.2 Comments

The idea of the IBL (Cebeci & Cousteix [4], Sychev et all. [48] and Le Balleur [25]) is to divide the flow into two regions : a boundary layer and an

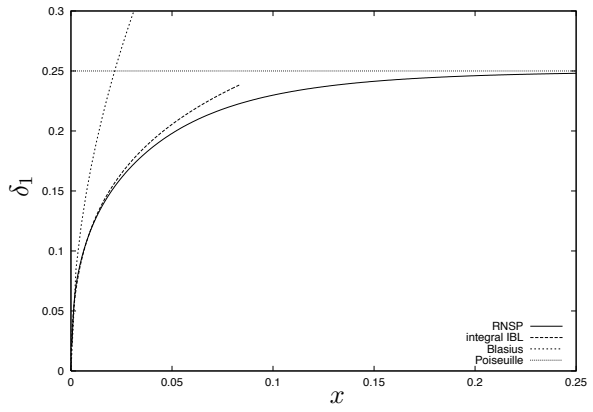

Figure 6: **Unconstricted situation : longitudinal evolution of the displacement thickness.** RNSP : numerical solution of the RNSP equations ; integral IBL : solution obtained with the integral IBL approach, rescaled in the x variable ; Poiseuille : $\delta_1 = 1/4$; Blasius : $\delta_1 = 1.7\bar{x}^{1/2}$.

inviscid core. The Boundary Layer equations are obtained in the same way as in the preceding paragraph which led to the Blasius solution. However, in the IBL case, an outer edge velocity $\bar{u}_e = \bar{u}(\bar{x}, \infty)$, corresponding to the velocity of the inviscid core, is introduced. The outer edge velocity is not necessarily equal to 1, as in the Blasius case. These two regions are strongly interacting, so that the radius seen by the inviscid core is no longer R_0^* but $R_0^*(1 - \varepsilon\bar{\delta}_1)$. The inviscid solution for a channel with a slow radius change is then obtained by a simple mass balance: $u^* = U_0^* \left[\frac{R_0^*}{R_0^*(1-\varepsilon\bar{\delta}_1)}\right]^2$, where $\bar{\delta}_1$ is the boundary layer displacement thickness.
In establishing the velocity displacement relation (Eq. 13), the key lies in the examination of the integral of the velocity over the channel cross-section. This integral is decomposed using a small parameter δ_ρ such as : $1 >> \delta_\rho >> \varepsilon$.

$$\int_0^1 (ru)dr = \int_0^{1-\delta_\rho} (ru)dr + \int_{1-\delta_\rho}^1 (ru)dr + (\int_{1-\delta_\rho}^1 (ru_e(\bar{x}))dr - \int_{1-\delta_\rho}^1 (ru_e(\bar{x}))dr).$$

When δ_ρ tends to 0, the combination of the first and third terms equals $\bar{u}_e/2$, as δ_ρ is located in the inviscid core where $u = \bar{u}_e$. The second and fourth terms may be recombined using the $\bar{y}$ boundary layer variable. As ε

tends to 0 faster than δ_ρ, *i.e.* $\delta_\rho/\varepsilon \to \infty$, their sum is :

$$-\varepsilon \int_{\delta_\rho/\varepsilon}^{0} ((1-\varepsilon\bar{y})\bar{u})d\bar{y} + \varepsilon(\int_{\delta_\rho/\varepsilon}^{0} ((1-\varepsilon\bar{y})\bar{u}_e(\bar{x}))d\bar{y}) \to -\varepsilon\bar{u}_e\bar{\delta}_1,$$

where $\bar{\delta}_1$ is the well known boundary-layer displacement thickness $\bar{\delta}_1 = \int_0^\infty (1 - \frac{\bar{u}}{\bar{u}_e(\bar{x})})d\bar{y}$. Finally, at order $O(\varepsilon^2)$: $\int_0^1 (ru)dr = \frac{\bar{u}_e}{2} - \varepsilon\bar{u}_e\bar{\delta}_1$, or :

$$\bar{u}_e(\bar{x})(1 - 2\varepsilon\bar{\delta}_1) = 1, \tag{14}$$

which may be rewritten as $\bar{u}_e(\bar{x})(1-\varepsilon\bar{\delta}_1)^2 + O(\varepsilon^2) = 1$ to be interpreted as mass conservation.
Note that the IBL description has terms of different order of magnitude because Eq. 14 degenerates into $\bar{u}_e(x) = 1$. The interaction between the boundary layer and the inviscid core disappears and the Blasius regime is recovered. This inconsistency does not appear in the pure Triple Deck description.
If a constriction of height ε and of length ε^2 (*i.e.* $f(x) = \varepsilon\bar{f}(\bar{x})$) is introduced, the new boundary condition at $\bar{y} = 0$ is : $\bar{u}(\bar{x}, \bar{f}(\bar{x})) = 0$ and $\bar{v}(\bar{x}, \bar{f}(\bar{x})) = 0$. Using the Prandtl transform : $\bar{x} \to \bar{x}$, $\bar{y} \to \bar{y} - \bar{f}(\bar{x})$ and $\bar{\delta}_1 = \int_0^\infty (1 - \frac{\bar{u}}{\bar{u}_e})d\bar{y}$, the problem reads again as (12), with a modified velocity displacement relation and an $O(\varepsilon^2)$ error :

$$\bar{u}_e(\bar{x})(1 - 2\varepsilon(\bar{\delta}_1 - \bar{f})) = 1, \tag{15}$$

with the former boundary condition at $\bar{y} = 0$ (*i.e.* $\bar{u}(\bar{x}, 0) = 0$ and $\bar{v}(\bar{x}, 0) = 0$).
As a conclusion, the IBL set of equations is encompassed by the RNSP(x) set at first order.

3.2.3 WSS

In dimensional form, the WSS is of order $O(\frac{\rho U_0^{*2}}{Re}\frac{\partial u}{\partial r})$, which leads to :

$$\tau^* = O(\varepsilon^{-1}\frac{\rho U_0^{*2}}{Re}). \tag{16}$$

3.2.4 The integral IBL solution

The IBL system (12, 13) may be simplified by integrating Eq. 12.2 over the transverse variable $\bar{y}$. The following integral system is obtained (see

Schlichting [38], Gersten & Hervig [12]) for the displacement thickness and the velocity for the inviscid core :

$$\frac{d}{d\bar{x}}(\frac{\bar{\delta}_1}{H}) = \bar{\delta}_1(1+\frac{2}{H})\frac{d\bar{u}_e}{d\bar{x}} + \frac{f_2 H}{\bar{\delta}_1 \bar{u}_e}, \qquad \bar{u}_e(\bar{x})(1-2\varepsilon\bar{\delta}_1) = 1, \qquad (17)$$

where H is the shape factor and f_2 is the friction coefficient.
To solve this system, a closure relationship linking H and f_2 to δ_1 and $\bar{u}_e$ is needed. By defining $\Lambda_1 = \bar{\delta}_1^2 \frac{d\bar{u}_e}{d\bar{x}}$, this closure relationship is obtained by locally approximating the velocity profile near the wall by a velocity profile of the Falkner Skan family (see Lorthois & Lagrée [23]) :

$$H = \begin{cases} H = 2.59e^{-0.37\Lambda_1} & \text{if } \Lambda_1 < 0.6 \\ H = 2.07 & \text{if } \Lambda_1 \geq 0.6 \end{cases}, \text{and} \quad f_2 = 0.94(-\frac{1}{H} + \frac{4}{H^2}). \quad (18)$$

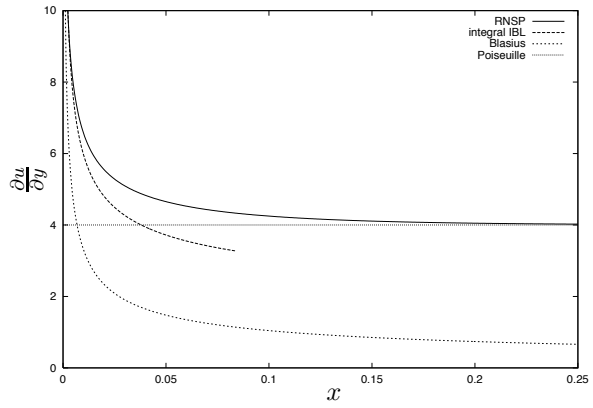

Figure 7: **Unconstricted situation : longitudinal evolution of the WSS.** RNSP : numerical solution of the RNSP equations ; integral IBL : solution obtained with the integral IBL approach, rescaled in the x variable ; Poiseuille : $\tau = 4$; Blasius : $\tau = 0.33x^{-1/2}$.

3.2.5 Numerical results for a straight pipe

Figs. 4 to 7 display the numerical solutions for the RNSP and IBL equations solved using an integral approach. For comparison, the IBL equations were solved at the RNSP scales. At these scales ($x = \varepsilon^2\bar{x}$ and $\delta_1 = \varepsilon\bar{\delta}_1$), the

integral system (17), becomes :

$$\frac{d}{dx}(\frac{\delta_1}{H}) = \delta_1(1+\frac{2}{H})\frac{d\bar{u}_e}{dx} + \frac{f_2 H}{\delta_1 \bar{u}_e}, \qquad \bar{u}_e(x)(1-2\delta_1) = 1. \tag{19}$$

Fig. 6 displays the evolution of the displacement thickness δ_1 obtained by the IBL integral method and its RNSP value deduced from the mass conservation relation (Eq. 14) e.g.: $\delta_1 = 1/2 - \int_0^1 ru/u(x,0)dr$, which is $1/4$ for the Poiseuille regime. Both solutions are superimposed for small x values ($x < 0.02$). For larger x, a discrepancy appears because the IBL description does not account for the opposite wall of the pipe. Therefore, the displacement thickness monotonically increases instead of reaching a finite asymptote of value $1/4$.
In addition, with the IBL approach, a first order correction to the Blasius regime near the entry in Blasius scales may be obtained. At first order in ε, the Blasius solution leads to $\bar{\delta}_1 \sim 1.7\bar{x}^{1/2}$ ([38]). Thus, from Eq. 13, $\bar{u}_e \sim 1 + 2\varepsilon 1.7\bar{x}^{1/2}$, which may be rewritten in $x = \varepsilon^2\bar{x}$ scales as: $\delta_1 = \varepsilon\bar{\delta}_1 \sim 1.7x^{1/2}$ and $\bar{u}_e \sim 1 + 3.4x^{1/2}$, valid for very small x. The associated pressure is then $\bar{p} \sim 3.4x^{1/2}$. These two asymptotes are respectively plotted on Figs. 4 and 5 and labelled as "Blasius cor". Note that the appearance of the $\sqrt{x}$ perturbation has been mentioned by Schlichting [38].
As displayed in Fig. 5, the longitudinal evolution of RNSP pressure behaves as the square root for small x and linearly for large x, suggesting a hyperbolic relationship. By least square regression :

$$p_{hyp} = -\frac{40}{53}\sqrt{(\frac{53x}{5}+1)^2 - 1}. \tag{20}$$

The maximal relative error for $0 < x < .2$ between Eq. 20, as plotted in Fig. 5, and the RNSP solution is 1.2%. Note that an additional error between the RNSP and NS solutions comes from the near entry effect and may be estimated from $(\rho_0 U_0^2)Re^{-1/2}$.
Finally, Fig. 7 displays the computed evolution of the WSS that starts from the Blasius asymptote $.33x^{-1/2}$ and goes to the constant Poiseuille value for large x as predicted by the theory.

3.3 RNSP(x): the link with Triple Deck and IBL

3.3.1 The Triple Deck Formulation

- LOWER DECK :
  After rescaling: $r = 1 - \varepsilon^2\tilde{y}$, $x = \varepsilon^2 + \varepsilon^5\tilde{x}$, $u = \varepsilon\tilde{u}$, $v = -\varepsilon^{-2}\tilde{v}$ and $p = \varepsilon^2\tilde{p}$ and assuming that $1 >> \varepsilon^5 >> Re^{-1}$ and a flat entry velocity profile, the RNSP(x) set leads to the final Triple Deck formulation as follows:

$$\frac{\partial\tilde{u}}{\partial\tilde{x}} + \frac{\partial\tilde{v}}{\partial\tilde{y}} = 0, \qquad (\tilde{u}\frac{\partial\tilde{u}}{\partial\tilde{x}} + \tilde{v}\frac{\partial\tilde{u}}{\partial\tilde{y}}) = -\frac{d\tilde{p}}{d\tilde{x}} + \frac{\partial^2\tilde{u}}{\partial\tilde{y}^2} \tag{21}$$

  with the following boundary conditions: $\tilde{u}(\tilde{x}, \tilde{f}(\tilde{x})) = 0$, $\tilde{v}(\tilde{x}, \tilde{f}(\tilde{x})) = 0$, $\tilde{u}(\tilde{x}, \tilde{y} \to \infty) \to (\frac{dU_{Blas}(0)}{d\bar{y}})(\tilde{y} + \tilde{A}(\tilde{x}))$ and the pressure displacement relation

$$\tilde{p}(\tilde{x}) = 2\tilde{A}(\tilde{x}) \tag{22}$$

  .

- MAIN DECK :
  The main deck scales are: $x = \varepsilon^2 + \varepsilon^5\tilde{x}$, identical to the lower deck longitudinal scale and $r = 1 - \varepsilon\bar{y}$, corresponding to the Blasius transversal scale. The velocity and pressure expand as:

$$u = U_{Blas} + \varepsilon u_{MD} + ... \qquad v = -\varepsilon^{-3}v_{MD} + ..., \qquad p = \varepsilon^2 p_{MD}, \tag{23}$$

  So that: $\frac{\partial u_{MD}}{\partial\tilde{x}} + \frac{\partial v_{MD}}{\partial\bar{y}} = 0$, $U_{Blas}\frac{\partial u_{MD}}{\partial\tilde{x}} + v_{MD}(\frac{dU_{Blas}(\bar{y})}{d\bar{y}}) = 0$ and $\frac{\partial p_{MD}}{\partial\bar{y}} = 0$, whose solution is: $u_{MD} = \tilde{A}(\tilde{x})(\frac{dU_{Blas}(\bar{y})}{d\bar{y}})$ and $v_{MD} = -\frac{d\tilde{A}}{d\tilde{x}}U_{Blas}$.

- UPPER DECK :
  The upper deck scales are: $r = r$, $x = \varepsilon^2 + \varepsilon^5\tilde{x}$ and velocity and pressure expand as :

$$u = 1 + \varepsilon^2 u_{UD} + ..., \qquad v = \varepsilon^{-3}v_{UD} + ..., \qquad p = \varepsilon^2 p_{UD} + ... \tag{24}$$

  So that: $\frac{\partial u_{UD}}{\partial\tilde{x}} + \frac{\partial r v_{UD}}{r\partial r} = 0$, $\frac{\partial u_{UD}}{\partial\tilde{x}} = -\frac{\partial p_{UD}}{\partial\tilde{x}}$ and $\frac{\partial p_{UD}}{\partial r} = 0$.

The boundary conditions for these two latter layers are obtained using asymptotic matching. They are presented in the following paragraphs.
Note that to be compatible with the Triple Deck scales, the constriction is redefined as $f = \varepsilon^2\tilde{f}(\tilde{x})$.

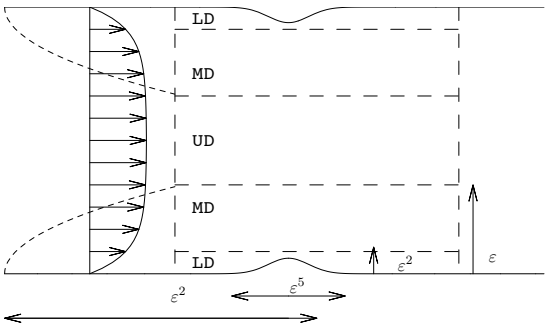

Figure 8: **Flow configuration in the Triple Deck case :** A mild constriction, of length ε^5 and height ε^2, is located at station ε^2, lying in the lower deck (LD). This thin layer is included in the boundary layer of thickness ε, or main deck (MD). The upper deck (UD) is the inviscid core.

3.3.2 Comments

The Triple Deck theory introduces a small perturbation to the Blasius regime, for which the thickness of the developed boundary layer is of order ε. The longitudinal scale of the location of the bump has thus to be of order ε^2, as deduced from the IBL formulation.
The upper deck, the main deck and the lower deck respectively corresponding to the inviscid core, the boundary layer of transverse scale ε and a small perturbed fraction of the boundary layer close to the wall (see Fig. 8).
Briefly, the approach of Ruban & Timoshin [34] is transposed to the axisymmetrical case. A constriction of small width x_3, such as $x = \varepsilon^2 + x_3\tilde{x}$, and of small height $\varepsilon_3\varepsilon$, such as $r = 1 - \varepsilon_3\varepsilon\tilde{y}$, is considered. It will be subsequently shown that $\varepsilon_3 = \varepsilon$ and that $x_3 = \varepsilon^5$. In the boundary layer (main deck), the longitudinal velocity is of order 1. Thus, the velocity slope $\partial u/\partial r$ is of order ε^{-1}. The velocity perturbation induced by a constriction of height $\varepsilon_3\varepsilon$ is then of order $((\varepsilon_3\varepsilon)\varepsilon^{-1}) = \varepsilon_3$. In the fraction $\varepsilon_3\varepsilon$ of the boundary layer, *i.e.* the lower deck, the balance of convection ($u\partial u/\partial x$) - diffusion ($\partial^2 u/\partial y^2$) leads to $x_3 = \varepsilon_3^3\varepsilon^2$. In the same way, the convection ($u\partial u/\partial x$) - pressure ($\partial p/\partial x$) balance shows that the pressure in the lower deck is of order ε_3^2.
As the lower deck equations give a velocity perturbation of order ε_3, the boundary layer velocity (main deck) must also be perturbed by an amount (ε_3), *i.e.* $u = U_{Blas} + \varepsilon_3 u_{MD}$. The perturbation of the Blasius regime is

simply solved from the RNSP equations in the main deck scales, showing that this perturbation is inviscid, and that $u = U_{Blas} + \varepsilon_3 \tilde{A}(\frac{dU_{Blas}(\bar{y})}{d\bar{y}})$ and $v = -(\varepsilon^{-1}\varepsilon_3^{-2})(d\tilde{A}/\tilde{x})U_{Blas}$. The function $-\tilde{A}$ represents the displacement of the stream lines in the boundary layer. For small $\bar{y}$, the longitudinal velocity may be expanded as : $(\frac{dU_{Blas}(0)}{d\bar{y}})\bar{y} + \varepsilon_3\tilde{A}(\frac{dU_{Blas}(0)}{d\bar{y}})$, or, in the lower deck variable ($\bar{y} = \varepsilon_3\tilde{y}$), as $\varepsilon_3\frac{dU_{Blas}(0)}{d\bar{y}}(\tilde{y} + \tilde{A})$. Hence, matching the velocity in the lower deck (*i.e.* $\varepsilon_3\tilde{u}$) for large $\tilde{y}$ with the velocity in the main deck for small $\bar{y}$ leads to :

$$\tilde{u} \to (\frac{dU_{Blas}(0)}{d\bar{y}})(\tilde{y} + \tilde{A}). \tag{25}$$

At the top of the main deck, where $U_{Blas} = 1$, the transverse velocity is $-(\varepsilon^{-1}\varepsilon_3^{-2})d\tilde{A}/d\tilde{x}$. This velocity is transmitted to the bottom of the upper deck and, by incompressibility, the longitudinal velocity perturbation u_{UD} is of order $\varepsilon_3\varepsilon$. The convection - pressure balance then shows that the pressure perturbation p_{UD} is also of order $\varepsilon_3\varepsilon$.
Finally, as the transverse pressure gradient is nul across the three layers, $\varepsilon_3\varepsilon$ is equal to the order of magnitude of the pressure in the lower deck, which is ε_3^2 (see above). Hence : $\varepsilon_3 = \varepsilon$ and $x_3 = \varepsilon^5$. In addition, the matching between the transverse velocity in the main deck for large $\bar{y}$ and the transverse velocity in the upper deck for r close to 1 leads to $v_{UD(r\to 1)} = -(d\tilde{A}/d\tilde{x})$. Since the upper deck is irrotational, which means that u_{UD} is independent on r, the transverse velocity is $v_{UD} = -(d\tilde{A}/d\tilde{x})r/2$. Thus, by incompressibility, $\partial u_{UD}/\partial\tilde{x} = -2d\tilde{A}/d\tilde{x}$. Finally, $p_{UD} = \tilde{p} = 2\tilde{A}$.
As a conclusion, the Triple Deck theory is included in the RNSP(x) set.
Another interpretation of $-\tilde{A}$ is that the flux relation (Eq. 13) is equivalent to the Triple Deck pressure deviation relation $\tilde{p} = 2\tilde{A}$. As done for obtaining Eq. 14, the displacement thickness is decomposed using a small parameter Y_1 such as $1 >> Y_1 >> \varepsilon$:

$$\bar{\delta}_1 = \int_0^{Y_1}(1-\frac{\bar{u}}{\bar{u}_e})d\bar{y} + \int_{Y_1}^{\infty}(1-\frac{\bar{u}}{\bar{u}_e})d\bar{y} - \int_0^{Y_1}(1-\frac{U_{Blas}}{\bar{u}_e})d\bar{y} + \int_0^{Y_1}(1-\frac{U_{Blas}}{\bar{u}_e})d\bar{y}. \tag{26}$$

In this case, $\bar{u}_e = U_{Blas}(\infty) = 1$. The combination of the first and third terms is evaluated in the lower deck where $\bar{u} = \varepsilon\tilde{u}$ and $\bar{y} = \varepsilon\tilde{y}$ as :

$$\int_0^{Y_1/\varepsilon}(1-\varepsilon\tilde{u})\varepsilon d\tilde{y} + \int_0^{Y_1/\varepsilon}(1-\varepsilon\tilde{y}(\frac{dU_{Blas}(0)}{d\bar{y}}))\varepsilon d\tilde{y}, \tag{27}$$

which is of order ε^2. The combination of the second and fourth terms is calculated when Y_1 approaches 0, *i.e.* in the main deck where $u = U_{blas} +$

$\varepsilon A(\frac{dU_{Blas}(\bar{y})}{d\bar{y}})$, so that the Blasius displacement thickness is reobtained plus a small term $-\varepsilon \int_0^\infty A(\frac{dU_{Blas}(\bar{y})}{d\bar{y}})d\bar{y}$ which equals $-\varepsilon A$. Therefore we obtain from Eq. 26:

$$\bar{\delta}_1 = \int_0^\infty (1 - U_{Blas})d\bar{y} - \varepsilon A + O(\varepsilon^2) = \bar{\delta}_{1,Blas} - \varepsilon A + O(\varepsilon^2). \qquad (28)$$

Linearization of Eq. 13 with this value of $\bar{\delta}_1$ gives a velocity perturbation of $-2\tilde{A}$, opposite to the pressure perturbation. Thus, the pressure deviation relation is $\tilde{p} = 2\tilde{A}$.
Note that the linearised solution of (21) may be obtained (see Gajjar & Smith [11]) and that, as no eigen function is found, the problem is parabolic. However, if ε is decreased to $Re^{-1/5}$, $x_3 = Re^{-1}$ and the constriction width equals the pipe diameter. Thus the RNSP(x) equations no longer hold because the upper deck fills up the entire pipe cross section and there is a transverse pressure gradient (see Smith [43]).
If the constriction is short, the influence of the opposite wall disappears. The Triple Deck with the pressure deviation law (Stewartson [45]):

$$p = \frac{1}{\pi} \int_{-\infty}^{\infty} \frac{A'}{x - \xi} d\xi,$$

is valid. This problem is not included in the RNSP(x) equations because the transverse pressure gradient has not been taken into account.
In conclusion, the Triple Deck equations are equivalent to the RNSP(x) equations (at first order) for all the relative scales:

$$Re^{-1/5} << \varepsilon << 1$$

3.3.3 WSS

The WSS τ^* is $O([\varepsilon^{-1}\frac{\rho U_0^2}{Re}])$, the same as the IBL scale.

3.3.4 Incipient separation : comparison with IBL.

The IBL equations (12, and 15), and the Triple Deck equations (21 and 22) were solved with the "semi inverse" method (Le Balleur [25]). This is an iterative process, iteration is done on δ_1 or $\tilde{A}$: the "Prandtl" part ((12.1-12.2) or (21)) is solved for the pressure with a finite difference scheme with δ_1 or $\tilde{A}$ imposed, then pressure displacement is solved for the pressure (15 or 22), the new value of δ_1 or $\tilde{A}$ is updated from the difference of pressures until convergence. The constriction shape is $\bar{f} = \alpha exp(-(2(K(\bar{x} - 1)/\bar{x}_l))^2$, with

$K = \sqrt{ln(2)}$ for the IBL and the integral IBL problems. The constriction $\tilde{f}$ is proportional to $exp(-(2(K(\tilde{x}-2)))^2$, with $K = \sqrt{ln(2)}$ for the Triple Deck problem. Fig. 9 displays the WSS at incipient separation, *i.e.* flow configuration where the WSS equals zero only at one point (the shear stresses are rescaled by the flat case). All the methods (RNSP, IBL, integral IBL and Triple Deck) show a good agreement, even if the slope discontinuity on the integral IBL curve, corresponding to the value $\Lambda_1 = 0.6$ where the derivative of H is discontinuous (Eq. 18) is visible. For a given boundary layer thickness ε^2, the value of α that promotes the incipient separation at different constriction widths $\bar{x}_l$ was numerically sought using the IBL equations. From the Triple Deck theory, α/ε is the relative perturbation in the lower deck, and it behaves like $\bar{x}_l^{1/5}$. As shown on Fig. 10 for $\varepsilon^2 = 10^{-3}$, this prediction is valid up to $\bar{x}_l = 0.3$.

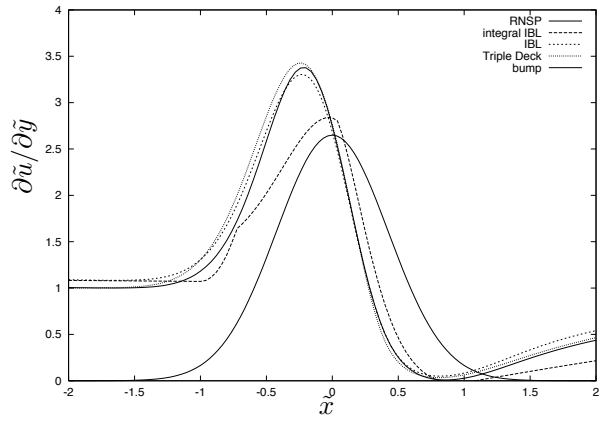

Figure 9: **Longitudinal evolution of the WSS near the incipient separation case** RNSP, integral IBL, full IBL resolution (in RNSP variables, the bump is located in $x = 0.02$, and its width is 0.00125), and Triple Deck resolution. All the curves are rescaled in Triple Deck scales.

3.4 RNSP(x): the link with Double Deck Equations

3.4.1 The Double Deck Formulation

- LOWER DECK :
  After rescaling: $r = 1 - \varepsilon 4^{-1/3}\check{y}$, $x = 1 + \varepsilon^3\check{x}$, $u = 4^{2/3}\varepsilon\check{u}$, $v =$

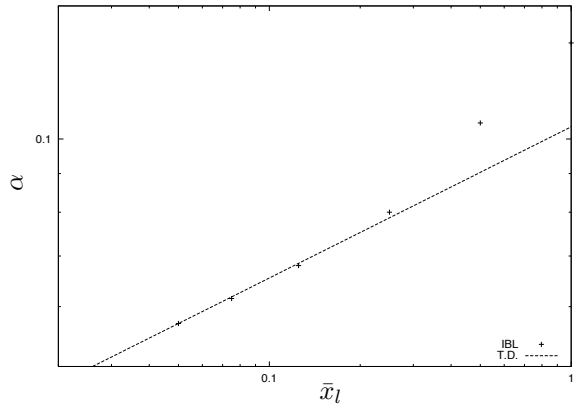

Figure 10: **Incipient separation : comparison between Triple Deck and IBL** : value of α that promotes the incipient separation versus the longitudinal width of the constriction $\bar{x}_l$ computed by the full IBL equations. The line of slope 1/5 (*i.e.* $\alpha \simeq \bar{x}_l^{1/5}$) is the Triple Deck prediction.

$-4^{1/3}\varepsilon^{-1}\check{v}$ and $p = 4^{8/3}\varepsilon^2\check{p}$ and assuming a Poiseuille entry velocity profile, the RNSP(x) set leads to the final Double Deck formulation as follows:

$$\frac{\partial \check{u}}{\partial \check{x}} + \frac{\partial \check{v}}{\partial \check{y}} = 0, \qquad (\check{u}\frac{\partial \check{u}}{\partial \check{x}} + \check{v}\frac{\partial \check{u}}{\partial \check{y}}) = -\frac{d\check{p}}{d\check{x}} + \frac{\partial^2 \check{u}}{\partial \check{y}^2} \tag{29}$$

with the following boundary conditions : $\check{u}(\check{x}, \check{f}(\check{x})) = 0$, $\check{v}(\check{x}, \check{f}(\check{x})) = 0$ and $\check{u}(\check{x}, \check{y} \to \infty) \to \check{y}$. Note that the Prandtl transform leads to $\check{u}(\check{x}, 0) = 0$, $\check{u}(\check{x}, \check{y} \to \infty) \to \check{y} - \check{f}(\check{x})$.

- MAIN DECK :
  The main deck scales are $x = 1 + \varepsilon^3\check{x}$, identical to the lower deck longitudinal scale, and $r = 1 - y$, corresponding to the Poiseuille transverse scale. Velocity and pressure expand as :

$$u = U_{Pois} + ..., \qquad v = 0 + ... \qquad p = 0 + ...$$

To be compatible with the Double Deck scales, the constriction is defined by $f = 4^{-1/3}\varepsilon\check{f}(\check{x})$.

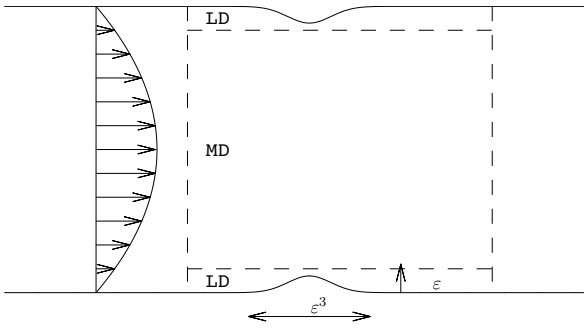

Figure 11: **Flow configuration in the Double Deck case :** A mild constriction is located at a station where a Poiseuille flow has developed. Its length is ε^3 and its height is ε, such as it lies in the lower deck (LD). The core flow is the main deck (MD).

3.4.2 Comments

The Double Deck theory introduces a small perturbation to the Poiseuille regime. In this theory, the flow is divided into two regions (see Fig. 11) : the fully viscous region (main deck) and a boundary layer of transverse scale $\varepsilon 4^{-1/3}$. The equations are directly obtained from Smith [41] or transposed from Saintlos & Mauss [37] to the axisymmetrical case. The matching condition $\check{u}(\check{x}, \check{y} \to \infty) \to \check{y}$ comes from the fact that the Poiseuille velocity in the core flow (main deck) is of value $U_{Pois} = 2(1 - r^2)$ but is $4^{2/3}\varepsilon\check{y}$ near the wall as ε tends to 0. This velocity must match the velocity at the outer edge of the lower deck (*i.e.* $4^{2/3}\varepsilon\check{u}(\check{x}, \infty)$). Note that the full Double Deck theory is directly derived from the NS description. In this description, the perturbations in the main deck have to be sought as :

$$u = 2(1 - r^2) + \varepsilon u_{MD} + ...; \qquad v = \varepsilon^{-2} v_{MD} + ...; \qquad p = \varepsilon^2 p_{MD} \tag{30}$$

Solving these perturbations either from the full NS or from the RNSP(x) equations leads to :

$$\frac{\partial u_{MD}}{\partial \check{x}} + \frac{\partial v_{MD}}{\partial y} = 0; \qquad (U_{Pois}\frac{\partial u_{MD}}{\partial \check{x}} + v_{MD}\frac{dU_{Pois}}{dy}) = 0 \tag{31}$$

However the development obtained for p_{MD} from the full NS description is :

$$U_{Pois}\frac{\partial v_{MD}}{\partial \check{x}} = -(\varepsilon^7) Re^2 \frac{\partial p_{MD}}{\partial y}. \tag{32}$$

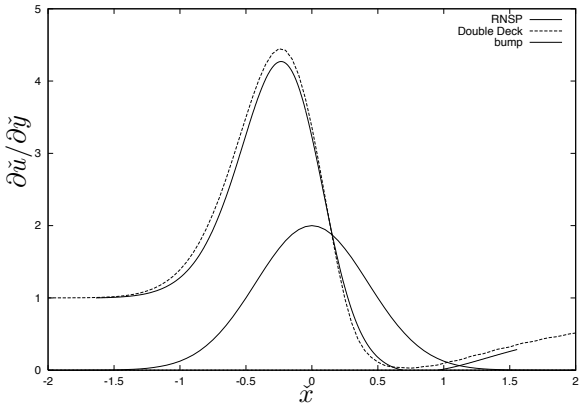

Figure 12: **Longitudinal evolution of the WSS near the incipient separation case** for $x_l = 0.0125$. D.D. : Double Deck resolution ; RNSP : RNSP resolution rescaled in Double Deck scales.

- First, the Double Deck theory requieres that ε is smaller than one. If $\varepsilon >> Re^{-2/7}$, Eq. 32 leads to $\frac{\partial p_{MD}}{\partial y} = 0$, which is consistent with the RNSP equations. In other words, if $\varepsilon >> Re^{-2/7}$ (or $Re\varepsilon^3 >> Re^{1/7}$), the RNSP(x) equations are equivalent to the Double Deck equations and the transverse pressure gradient is not relevant.

- Second, when $\varepsilon = Re^{-2/7}$, corresponding to real constriction length $R_0^* Re^{1/7}$ and height $R_0^* Re^{-2/7}$, the RNSP(x) is no longer valid. However, it may be shown that the pressure drop is linked to the second derivative of the displacement function $\check{A}$. In particular, in the symmetrical case, it may be shown (Smith [41]) that $v_{MD} = 0$ (so $\check{A} = 0$) . This is why the RNSP(x) set remains valid for symmetric case even if $\varepsilon = Re^{-2/7}$.

- Third, if $\varepsilon << Re^{-2/7}$, from Eq. 32, the equation at first order of ε is $\frac{\partial v_{MD}}{\partial \check{x}} = 0$ and its solution $v_{MD} = 0$. Thus, perturbations appear at higher orders. Consequently, $\frac{\partial p_{MD}}{\partial y} = 0$. The value $\varepsilon = Re^{-1/3}$, at which the physical longitudinal scale is R_0^*, is included in this scenario.

- Finally at short scale when the variations of x^* and y^* are of same order, a full NS problem is encountered. This corresponds to $\varepsilon^3 Re R_0^* = \varepsilon R_0^*$. Thus, for the Double Deck equations to hold, ε must be greater

than $Re^{-1/2}$.

In conclusion, the Double Deck equations are equivalent to the RNSP(x) equations (at first order) for all the relative scales:

$$Re^{-1/2} << \varepsilon << 1$$

3.4.3 WSS

The skin friction τ^* is $O(4(\rho U_0^{*2}/Re))$ for a constriction of physical length $R_0^* < \varepsilon^3 Re R_0^* << R_0^* Re^{1/7}$ and of height εR_0^*.

3.4.4 Incipient separation : comparison with RNSP

Starting from a Poiseuille flow, a constriction $R(x) = 1 - \alpha exp(-(2K(x - x_c)/x_l)^2)$, with $exp(-K^2) = 0.5$, was introduced, which corresponds to $\check{f}(\check{x}) = \alpha_{D.D.} exp(-(2K\check{x})^2)$ in the Double Deck description. The equation is the same as in the Triple Deck case, but the scales are different.
Fig. 12 displays the WSS near incipient separation, showing a good agreement between the RNSP and the Double Deck solutions in the case of a small constriction.
Then, the value of α that promotes incipient separation for incrasing constriction widths x_l was numerically sought using the RNSP equations. Fig. 13 displays the value of α, denoted α_{IS}, as a function of x_l. As expected from the Double Deck theory, which implies that :

$$\alpha_{IS} = \alpha_{D.D.,IS}(4^{-1/3})(x_l)^{1/3}, \tag{33}$$

where $\alpha_{D.D.,IS}$ is the unique Double Deck incipient separation angle, α_{IS} behaves as $x_l^{1/3}$. Numerical resolution of the Double Deck equations led to $\alpha_{D.D.,IS} \simeq 2.0$. The curve $2.(4^{-1/3})(x_l)^{1/3}$ is referred as "D.D." on Fig. 13.

3.4.5 Maximum value of WSS for a given constriction

Finally, increasing the constriction angle in the Double Deck scales, with $6 > \alpha_{D.D.} > 0$, the maximum value of the WSS is fitted as :

$$1.11 + 0.984\alpha_{D.D.} + 0.28\alpha_{D.D.}^2. \tag{34}$$

Expressing $\alpha_{D.D.}$ as a function of x_l and α in Eq. 34 and multiplying by $4(\rho U_0^2/Re)$, the asymptotic maximum WSS obtained in the case of a small

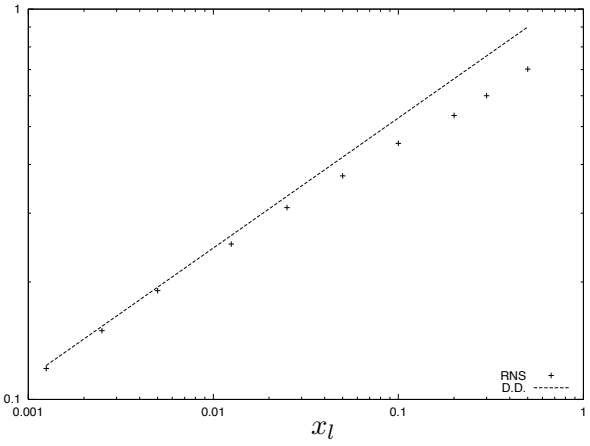

Figure 13: **Incipient separation : comparison between Double Deck and RNSP** : value of α which promotes the incipient separation versus the longitudinal width of the constriction x_l computed by the RNSP approach. The line of slope 1/3 (*i.e.* $\alpha \simeq x_l^{1/3}$) is the Double Deck prediction.

constriction is thus given by :

$$4(\rho U_0^2/Re)(1.11 + 0.984\frac{4^{1/3}\alpha}{x_l^{1/3}} + 0.28\frac{4^{1/3}\alpha^2}{x_l^{1/3}}) \tag{35}$$

3.5 RNSP(x): the link with quasi Poiseuille flow

After rescaling $x = Xx'$, with $X >> 1$, $r = r'$, $v = X^{-1}v'$ and $p = Xp'$, the RNSP(x) set leads at first order in X^{-1} to the classical quasi Poiseuille flow: each velocity profile is a Poiseuille one. The well known relation for the WSS is obtained (for extremely large constrictions *i.e.* larger than $R_0^* Re$ in physical scales):

$$\tau^* = 4(\rho U_0^{*2} Re^{-1})(\frac{R_0^*}{R^*(x)})^3 \tag{36}$$

3.6 RNSP(x): the link with another IBL case

3.6.1 Final Formulation

After rescaling $r = R(\overline{\overline{x}}) - (\lambda/Re)^{-1/2}\ \overline{\overline{y}}$, $u = \overline{\overline{u}}$, $v = -(\lambda/Re)^{1/2}\ \overline{\overline{v}}$, $x - x_b = (\lambda/Re)\ \overline{\overline{x}}$ and $p = \overline{\overline{p}}$, where x_b is the position of the constriction throat and λR_0^* the width of the throat, the RNSP(x) set leads to the final IBL (Interacting Boundary Layer) formulation as follows:

$$\frac{\partial\ \overline{\overline{u}}}{\partial\ \overline{\overline{x}}} + \frac{\partial\ \overline{\overline{v}}}{\partial\ \overline{\overline{y}}} = 0, \qquad (\overline{\overline{u}}\ \frac{\partial\ \overline{\overline{u}}}{\partial\ \overline{\overline{x}}} + \overline{\overline{v}}\ \frac{\partial\ \overline{\overline{u}}}{\partial\ \overline{\overline{y}}}) = \overline{\overline{u}}_e\ \frac{d\ \overline{\overline{u}}_e}{d\ \overline{\overline{x}}} + \frac{\partial^2\ \overline{\overline{u}}}{\partial\ \overline{\overline{y}}^2}, \tag{37}$$

$$\overline{\overline{u}}_e = \frac{1}{(R^2 - 2(\lambda/Re)^{-1/2}\ \overline{\overline{\delta}}_1)}, \tag{38}$$

where $\overline{\overline{\delta}}_1 = \int_0^\infty (1 - \frac{\overline{\overline{u}}}{\overline{\overline{u}}_e}) d\ \overline{\overline{y}}$, and with the following boundary conditions : $\overline{\overline{u}}\ (\overline{\overline{x}}, 0) = 0$, $\overline{\overline{v}}\ (\overline{\overline{x}}, 0) = 0$ and $\overline{\overline{u}}\ (\overline{\overline{x}}, \infty) = \overline{\overline{u}}_e$.

3.6.2 Comments

The constriction throat is located at station x_b, and is of relative length in RNSP (λ/Re). The equations are almost identical to equations (12, 13) in the IBL section (§3.2.1) except the flux conservation relation (Eq. 38). In the previous IBL section, the transition from a flat profile to a Poiseuille profile has been discussed. In a severe constriction the opposite occurs : the Poiseuille profile becomes a flat profile associated with an inviscid core. The IBL formulation again applies, but new scales have to be introduced (see Lorthois & Lagrée [23], Lorthois et al. [24]). This will be numerically verified in the following section where the RNSP(x) solution shows a flat profile at the throat for any given entry profile.

3.6.3 WSS

Using this IBL point of view, an heuristical evaluation of the WSS may be found. If the relative aperture of the constriction $1 - \alpha$ is small, *i.e.* $(1 - \alpha) << 1$, the order of magnitude of the velocity obtained by flux conservation increases from 1 at the pipe inlet to $1/(1 - \alpha)^2$ at the constriction throat. If λR_0^* represents the constriction length, R_0^* the common scale in x and y and Re the Reynolds number , the transverse velocity scale in the boundary layer is then $(1 - \alpha)\lambda^{1/2} Re^{-1/2}$.

The displacement thickness is then

$$\delta_1 = d_1(1-\alpha)\lambda^{1/2}Re^{-1/2}, \tag{39}$$

where d_1 is an $O(1)$ numerical value. The first correction to the velocity is from the displacement thickness δ_1, whose effect is to increase the constriction felt by the inviscid core. The velocity is thus sligthly greater than $(1-\alpha)^{-2}$ and may be evaluated by $(1-\alpha-\delta_1)^{-2}$. As $\lambda^{1/2}Re^{-1/2} << 1$, Eq. 13 leads to the following approximation for the velocity :

$$u = (1 + 2d_1((Re/\lambda)^{-1/2}))(1-\alpha)^{-2}. \tag{40}$$

The displacement thickness corrected by this extra acceleration is :

$$\delta_1 = d_1(1-\alpha-d_1(1-\alpha)\lambda^{1/2}Re^{-1/2})\lambda^{1/2}Re^{-1/2}. \tag{41}$$

Finally, the WSS at the constriction throat may be approximated as the ratio of Eq. 40 and Eq. 41 divided by 4, which is the Poiseuille WSS :

$$WSS = (\mu\frac{\partial u^*}{\partial y^*})/((\mu\frac{4U_0^*}{R^*})) \sim .22\frac{((Re/\lambda)^{1/2}+3)}{(1-\alpha)^3} \tag{42}$$

The numerical coefficient .22 is based on the assumption that flow acceleration at the constriction throat corresponds to the value of a convergent channel (see Gersten & Hervig [12] or Schlichting [38] and §3.2.4 for the definition of H and f_2), for which $Hf_2/4 \sim .22$. In addition, it is assumed that $d_1 \sim 1$. Note that details on the integral method and closure relationships may be found in Lorthois & Lagrée [23]. The constriction recreates an interacting boundary layer flow. Therefore, the relevant Reynolds number is no longer Re but $Re\lambda$ and $(Re/\lambda)^{1/2}$ is the inverse of the relative boundary layer thickness.

3.6.4 Comparison with NS and RNSP(x)

- Comparison with NS :
  Siegel et al. [40] have numerically solved the NS equations in a constricted pipe. Based on their results, they postulated an *ad hoc* dependence for the maximal WSS as:

  $$WSS_{max,Sieg} = aRe^{1/2} + b \tag{43}$$

  where coefficients a and b were dependent on the constriction geometrical parameters α and λ. On the contrary, the IBL approach led

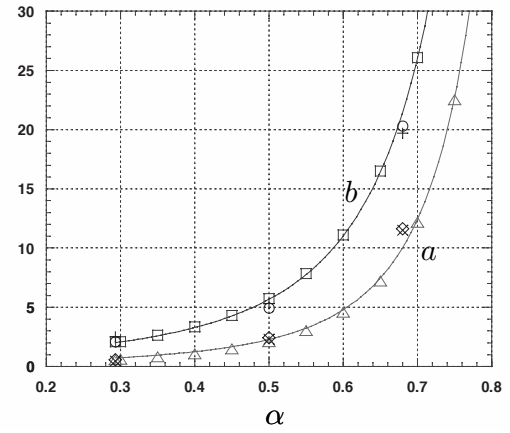

Figure 14: **Coefficient a and b for the maximum WSS** (see Eq. 43). $\diamond$: coefficient a derived from Siegel for $\lambda = 3$; $\times$: coefficient a derived from Siegel for $\lambda = 6$; $\bigcirc$: coefficient b derived from Siegel for $\lambda = 3$; $+$: coefficient b derived from Siegel for $\lambda = 6$. Coefficients a ($\triangle$) and b ($\square$) obtained using the IBL integral method ; solid lines : Coefficients a and b from Eq. 44.

to the universal scaling law Eq. 42. This heuristical scaling law has first been numerically tested by solving the IBL system using an integral formulation. The regression analysis of the numerical results for various shapes led to :

$$WSS_{max} = (\mu \frac{\partial u^*}{\partial y^*})/((\mu \frac{4U_0}{R})) \sim .231(\frac{(Re/\lambda)^{1/2}}{(1-\alpha)^{3.311}} + \frac{3.11}{(1-\alpha)^{2.982}}) \tag{44}$$

Note that the coefficients are very close to the theoretical ones (see Eq. 42), and they show very good agreement with the numerical values derived from Siegel et al. (1994) (see Fig. 14).

- Comparison with RNSP(x):
  The set of RNSP(x) equations has been solved by the marching finite-differences scheme. Fig. 15 displays the evolution of the velocity profile along the convergent part of a 70% constriction, for two different imposed entry profiles: a flat profile (fully potential entry) and a Poiseuille profile (fully viscous entry). As expected, when the entry flow is fully viscous, strong flow acceleration causes the velocity profile

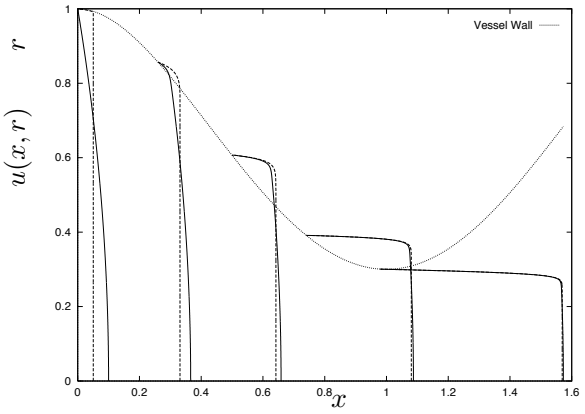

Figure 15: **Evolution of the velocity profile along the convergent part of a 70% stenosis** computed using the RNSP approach, with $Re = 500$; solid line: Poiseuille entry profile; broken line: flat entry profile.

to flatten. At the constriction throat, the flow is thus independent of the entry velocity profile. In particular, the maximal WSS is in good agreement (3% discrepancy) with the maximal WSS obtained by the IBL scaling law (Eq. 44) (see Fig. 16). In conclusion, the described set of RNS equations is "fully interactive" without any matching step and well suited for studying flow fields in constrictions.

Siegel et al. [40] and Huang et al. [14] have numerically solved Navier-Stokes equations for $100 < Re < 1000$. The results obtained are consistent with our method. Furthermore, the bidimensional counterpart of this RNSP and IBL theories has been settled in Lagrée et al. [21]. Some comparisons have been done with a NS solver focusing on the pressure $p(x)$ and on the reverse flow. It has been observed that for Re from 100 to 1000, IBL, RNSP, and NS give very similar results.

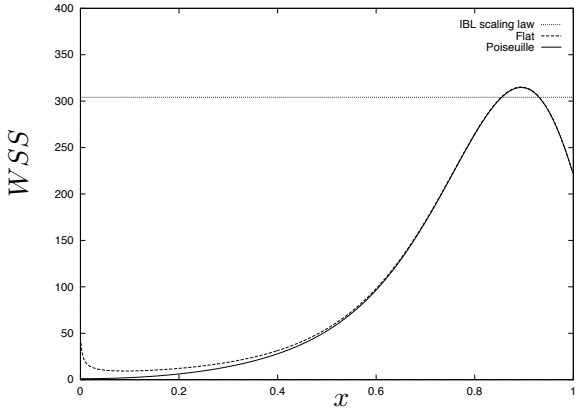

Figure 16: **Longitudinal evolution of the WSS along the convergent part of a 70% stenosis** computed using the RNSP approach with $Re = 500$; solid line: Poiseuille entry profile ; broken line: flat entry profile.

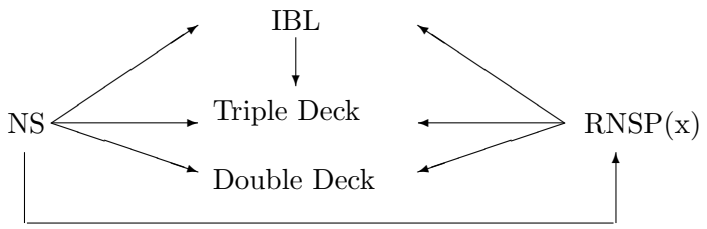

Figure 17: **The different models**: RNSP is obtained from Navier Stokes (NS). Triple Deck, Double Deck and IBL are obtained from NS, they may be obtained from RNSP in the pipe flow considered .

4 Conclusion

model	RNSP	IBL	IBL	Triple Deck	Double Deck
section	§2.2	§3.2.1	§3.6.1	§3.3	§3.4
Initial prof.	any	Blasius	any	Blasius	Poiseuille
bump pos.	$x = O(1)$	$x = O(\varepsilon^2)$	any	$x = O(\varepsilon^2)$	$x > 1$
bump width	any	ε^2	$O(1/Re)$	ε^5	ε^3
bump height	any	ε	$O(1)$	ε^2	ε
validity	$Re >> 1$	$Re^{-1/2} \ll \varepsilon \ll 1$	$Re >> 1$	$Re^{-1/5} \ll \varepsilon \ll 1$	$Re^{-1/2} \ll \varepsilon \ll 1$

Table 1: The scales may be tabulated in the following table (longitudinal length are scaled with $R_0^* Re$, transverse are scaled by R_0^*.

Having in mind applications in biomechanics, where the elevated wall shear stresses encountered in arterial stenoses are likely to play a role in the mechanisms of thrombo-embolism and atherosclerotic plaques ruptures, the purpose of this study is to evaluate the scale of the wall shear stress τ^* in a constricted pipe. Of course, the computation of such flows is now accurately achieved through Navier-Stokes solvers in a reasonable range of Reynolds numbers. On the other hand, simplified 1D theories and correlations from experimental data are available. Our work fills the gap between them. We claim that the asymptotic equations provide a better understanding of flow structure and of the relevant scalings as well. As computational time is reduced, parameters may be easily changed and their influence can be analysed. Thus, in this paper, we have presented a system that we call RNSP, referring to the Reduced Navier-Stokes equations, which are in fact

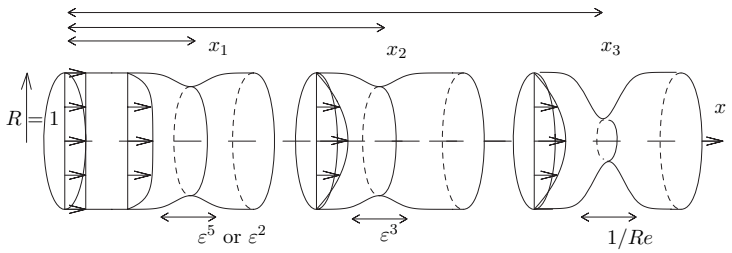

Figure 18: **Flow configurations :** A constriction may be located at $x_1 = O(\varepsilon^2)$ where an inviscid fluid core still exists; if the width is ε^2 IBL applies (§3.2.1). If the width is ε^2 the Triple Deck applies (§3.3). A constriction may be located at $x_2 > 1$ where the Poiseuille profile has developed, but the width has to be ε^3 for Double Deck (§3.4). If the constriction is short, but severe enough, IBL applies (§3.6.1).

the Prandtl equations with different boundary conditions. We have shown how to obtain the RNSP system from the NS system. Then, we have established the connection between the RNSP system and many other asymptotic descriptions of the Navier-Stokes equations, as summarised on Fig. 17, 18, and Table 1:

- First, the IBL equations deduced from the RNSP have been discussed. The entry effect has been computed using both the RNSP equations and a simple integral IBL description. They show a good agreement.
- We compared a full IBL resolution to a Triple Deck solution in the case of a very small constriction, located in the vicinity of a fully potential entry. The constriction height that promotes incipient separation was calculated using both Triple Deck theory and the IBL description.
- Then, the RNSP equations was compared with the Double Deck equations in the case of a small reduction of the pipe radius, assuming a fully viscous entry. The constriction height that promotes incipient separation was calculated using both the Double Deck theory and the RNSP description.
- A case of extremely long bumps leading to a Poiseuille flow was presented.

- Finally, a case where the initial potential flow is destroyed, leading to an IBL flow, has been studied. Maximum skin friction was calculated using simple IBL arguments. This permitted us to obtain an universal scaling law for the WSS.

A selected number of examples have been presented. Note that the gain in computational time is significant when compared with a full NS solution. Dimensional scaling allows a better understanding of various physical phenomena. In each section, the limits of the asymptotic descriptions was presented. The most interesting conclusion is that the transverse pressure gradient is irrelevant in a large number of cases. Thus, the flow in a constricted pipe is mainly "parabolic": the disturbances propagate downstream and weakly upstream which allows marching computation (see [21] for a comparison between RNSP/ IBL and full NSin case of reverse flow in a bidimensional configuration). In addition, the independence of the flow on the entry velocity profile has great implications because the *in vivo* entry profile is unknown and not parabolic as assumed in most studies.
In conclusion, it has been verified asymptotically and numerically that, in the pipe case, the RNSP(x) system agrees with most of the Double/ Triple Deck sets of equations and the IBL as well. Thus, the RNSP system may be used in cases of stenotic pipes. The bidimensional extension is straightforward. Extension to unsteady and non-axisymetrical flows is currently in progress.

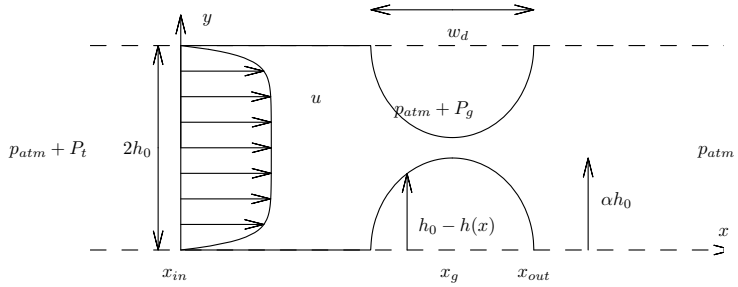

Figure 19: The obstacles are two half-circles of width $w_d = 2R_g$ and of height $R_g = \alpha h_0$ (the channel half height is h_0). The flow is induced by the pressure drop P_t from a pressure reservoir (at the left). The out flow creates a jet in an room at pressure p_{atm}. Pressure is measured at the throat $p_{atm} + P_g$, that is this pressure that we want to predict.

Part II
2D Case

We use again our strong approximations: the flow is supposed to be 2D, laminar, and steady. In this framework we will cross compare numerical resolution of the Navier Stokes equations (NS) and resolution of two asymptotic models (Sychev *et al.* [48]). Those two models are first, the Interacting Boundary Layer theory (IBL) which is the boundary layer theory with a strong coupling with the ideal fluid and second, a simplified "reduced" set of Navier Stokes equations (RNSP). We will see that these three approaches give nearly the same results, comparisons with experiments will show the limits of the hypotheses as the flow becomes turbulent in the jet region.

5 Equations

5.1 Navier Stokes

In order to non-dimensionalize the Newtonian steady laminar incompressible bidimensional Navier Stokes equations (NS), we use U_0 the entry velocity for the velocities, h_0 for the lengths, ρU_0^2 for variations of pressures. The Reynolds number is $Re = U_0 h_0/\nu$. As boundary conditions, we impose a flat entry velocity profile of value $(\bar{u}(0,\bar{y}), \bar{v}(0,\bar{y})) = (1,0)$ (a Poiseuille one with maximal value $\frac{3}{2}$ gives the same results) and zero velocity on the

wall (the bump is centered in $\bar{x}_g$). We impose symmetry condition on the axis $\bar{y} = 0$: $\partial\bar{u}(\bar{x}, 0)/\partial\bar{y} = 0$ and $\bar{v}(\bar{x}, 0) = 0$. A zero constant pressure is imposed at exit $\bar{p}(\bar{x}_{out}, \bar{y}) = 0$, this latter condition corresponding to a simple implementation of an open boundary condition (Gresho [13]). The system is solved with the numerical finite element code Castem 2000 [29] on a mesh of quadrangles (80 x 16 vertices). The computed value of the pressure at the entrance ($\bar{p}(\bar{x}_{int}, \bar{y})$) allows then to evaluate the total pressure drop.

5.2 Reduced Navier Stokes/ Prandtl Equations

The results have been compared to a first kind of simplification obtained from Navier Stokes equations by supposing that the transverse scale is the width of the channel h_0 itself and that this scale is smaller than the longitudinal one. Supposing that the Reynolds number is large, we neglect some viscous effects and consider only longitudinal variations of pressure. We do it in a boundary layer theory spirit (Gersten [12]), we recover Prandtl equations but with different boundary conditions. The main differences are first, that the transverse variable is bounded, which is not the case in boundary layer theory where we have to match "at infinity" with the ideal fluid and second, that the pressure is not given by the ideal fluid but is a result of the computation. So, because these equations may as well be seen as a reduced system obtained from Navier Stokes equations, we call this system RNSP (Reduced Navier Stokes/ Prandtl).

To settle the equations, u is scaled by U_0, v by U_0/Re, x by $h_0 Re$, y by h_0, and p by ρU_0^2, with Reynolds number $Re = U_0 h_0/\nu$, which is assumed large. The flow is supposed quasistatic: the Strouhal number is low and the spatial acceleration is large. We obtain:

$$\frac{\partial}{\partial\tilde{x}}\tilde{u} + \frac{\partial}{\partial\tilde{y}}\tilde{v} = 0, \qquad \tilde{u}\frac{\partial}{\partial\tilde{x}}\tilde{u} + \tilde{v}\frac{\partial}{\partial\tilde{y}}\tilde{u} = -\frac{\partial}{\partial\tilde{x}}\tilde{p} + \frac{\partial^2}{\partial\tilde{y}^2}\tilde{u}, \qquad 0 = -\frac{\partial}{\partial\tilde{y}}\tilde{p}. \quad (45)$$

The boundary conditions are: no slip $\tilde{u}(\tilde{x}, \tilde{y} = \tilde{h}(\tilde{x})) = 0$, $\tilde{v}(\tilde{x}, \tilde{y} = \tilde{h}(\tilde{x})) = 0$ at the upper wall defined by $\tilde{h}(\tilde{x})$ (whose dimension is h_0) and symmetry ($\partial_{\tilde{y}}\tilde{u}(\tilde{x}, \tilde{y} = 0) = 0$, $\tilde{v}(\tilde{x}, \tilde{y} = 0) = 0$). At the entrance, the pressure is zero and the first velocity profile is given, for example a flat profile $\tilde{u} = 1$, $\tilde{v} = 0$. As long $\tilde{u} > 0$, the system is marching in $\tilde{x}$ (or parabolic), there is no outflow condition. The system is solved with finite differences (2500 * 1000 points) and at each station $\tilde{x}$ one has to find by a Newton iteration the value of the pressure $\tilde{p}(\tilde{x})$ for the fitting of the boundary condition for $\tilde{v}$. The total pressure drop is a result of the computation.

5.3 Integral IBL

The Integral Interacting Boundary Layer equations (IBL) may be deduced from Navier Stokes equations (or from those RNSP equations) supposing that the Reynolds number is large and that viscous effects are restricted to a thin layer near the wall. We simplify further the Prandtl boundary layer equations by using the integral von Kármán equation (Schlichting [38]), and with the same previous scales, this gives the following coupled system (46). This interacting system may be understood as follows.

First, the ideal fluid promotes the variations of the boundary layer and more precisely the variations of the boundary layer displacement thickness $\tilde{\delta}_1$.

Second, in growing, the displacement thickness $\tilde{\delta}_1$ retroacts on the ideal fluid through the flux conservation.
The two equations are strongly coupled and are solved with the Le Balleur [25] "semi-inverse" method.

$$\frac{d}{d\tilde{x}}(\frac{\tilde{\delta}_1}{H}) + \frac{\tilde{\delta}_1}{\tilde{u}_e}(1+\frac{2}{H})\frac{d\tilde{u}_e}{d\tilde{x}} = \frac{f_2 H}{\tilde{\delta}_1 \tilde{u}_e}, \qquad \tilde{u}_e(\tilde{x}) = \frac{1}{\tilde{h}(\tilde{x}) - \tilde{\delta}_1(\tilde{x})}. \quad (46)$$

Initial condition are for example $\tilde{\delta}_1(0) = 0$ and $\tilde{u}_e(0) = 1$. To solve this system, a closure relationship linking the shape function H and friction function f_2 to the velocity and the displacement thickness is needed. Defining $\Lambda_1 = \tilde{\delta}_1^2 \frac{d\tilde{u}_e}{d\tilde{x}}$, the system is closed from the resolution of the Falkner-Skan system as follows:,

$$H = \left\{ \begin{array}{ll} 2.5905 e^{-0.37098\Lambda_1}, & \text{if } \Lambda_1 < 0.6 \\ 2.074, & \text{if } \Lambda_1 > 0.6 \end{array} \right\}, \qquad f_2 = 1.05(-H^{-1} + 4H^{-2}).$$

This closure allows flow separation for decelerated flows. Those simplifications are in the spirit of Lorthois *et al.* [24], but here 2D. Kalse *et al.* [15] used recently nearly the same modelisation. As a result, the pressure is computed by Bernoulli law from the computed velocity $\tilde{u}_e(\tilde{x})$.

We compare then the NS results with the RNSP and IBL results. Examples are represented on Figures 20 and 21 where we used R_g as longitudinal scale to plot the curves; numerically in (50) and (46), the radius is of length $R_g/(h_0 Re)$. Of course, this length is finite and small in the computations which are done for a finite value of the Reynolds number.

6 Numerical results: relative pressure drops

Some computations have been done on various geometries: on circles, on ellipses, on exponential walls, or on arcs of sine. It has been observed that the IBL, RNSP, and NS results were the same (in the range $0 < \alpha < 0.8$, $100 < Re < 1000$). For larger values of α, the boundary layer thickness at the throat is very thin, as is seen below Eq. 47. So, NS needs a careful mesh refinement near the wall that we did not attempt to do, because we preferred to focus on the simplified problems. For those values of α close to 1, IBL and RNSP nevertheless give the same results. As the acceleration is large in the stenosis, the solution does not depend on the initial velocity profile (nor on the value of $\tilde{\delta}_1(0)$). Iso pressures computed by Navier Stokes are "sufficiently" close to perpendiculars to the axis to justify RNSP description. We observed that the pressure distribution at the wall has nearly always the same shape, seen on Figure 20, on a moderate case of degree of stenosis of $\alpha = 0.75$ and $Re = 500$. This pressure curve has a well known shape: a pressure drop at the throat and recompression with a plateau due to the jet. As expected, we obtain the order of magnitude of the size of the recirculation after the cylinders: $h_0 Re$. Figure 20 is a comparison between the pressures computed by IBL, RNSP, and NS; the larger arrow represents the maximal pressure drop $\tilde{P}_m$, the second arrow (in size) represents the pressure drop between output and input ($\tilde{P}_t > 0$), and the smaller arrow represents the pressure drop between the throat (where $\tilde{P}_g < 0$) and the output.

We observed that cutting the computation domain in the downstream jet (i.e. where flow separation occurs) is not a problem for Castem (in the range used, $0 < \alpha < 0.8$, $100 < Re < 1000$); so downstream seems to have a negligible influence on upstream. For the RNSP system, the resolution is done in marching in x, and so, the flow at station x ignores downstream conditions. RNSP equations present nevertheless a difficulty in the separated flow region: there is an intrinsinc numerical instability due to the negative velocity which causes trouble if the separation bulb is too large, as is the case here. Consequently, we use the so-called FLARE approximation which consists in removing the $u\partial u/\partial x$ term when u is negative, preventing any downstream information and allowing separation to be computed. We observed that if the discretization step is too small, numerical problems reappear. Nevertheless, as all the curves are nearly the same, the FLARE approximation is here validated by the full Navier Stokes computation and by the IBL computation where Falkner-Skan profiles were computed without approximation.

This very weak influence of downstream on upstream may be understood

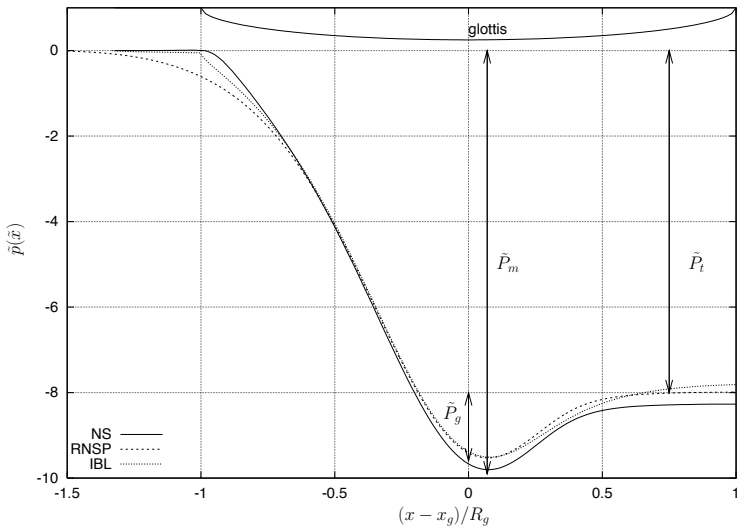

Figure 20: A comparison between computed non-dimensional pressure for the three models (NS, IBL and RNSP, in this last case the wall has been smoothed in $x = \pm 1$ to avoid an infinite slope, this was not the case for NS and IBL), here $\alpha = 0.75$, $Re = 500$. The upper half geometry is plotted as well (the smoothed one is not plotted). It is observed that the ratio: pressure at the glottis divided by maximum pressure drop is nearly constant ($K_e = \tilde{P}_t/\tilde{P}_m \simeq 0.82$). Likewise, the ratio: pressure at the output divided by the pressure drop betwen the output and the glottis is nearly constant ($K_t = \tilde{P}_t/(\tilde{P}_t - \tilde{P}_g) \simeq 0.86$).

because, as already mentioned, the equations (50) are parabolic in x (if $u > 0$). The IBL equations (46) may be solved with a streamwise marching as well (this result is not obvious and depends of the kind of interaction between the boundary layer and the perfect fluid, Le Balleur [25]; ultimate justifications are linked with the Triple Deck theory). IBL equations allow to compute flow separation.

Even with those approximations, NS, RNSP, and IBL give very similar results. Computational time is of course far shorter for the RNSP and IBL than for NS.

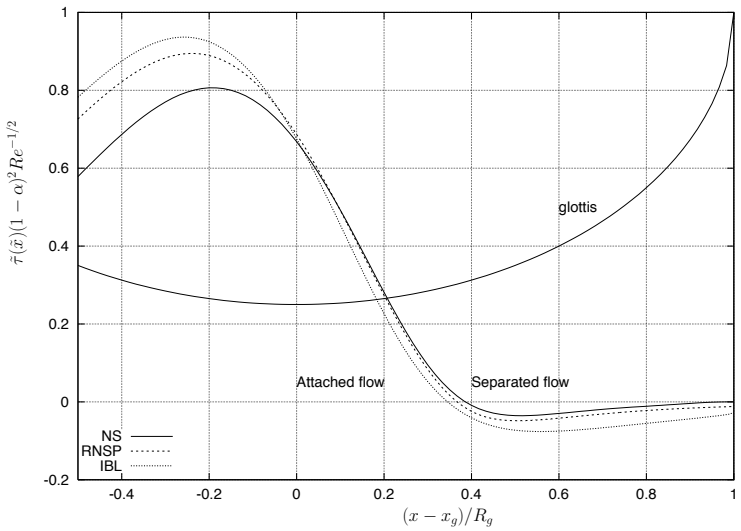

Figure 21: A comparison between computed skin friction divided by $(0.47 * 2.07)(1-\alpha)^{-1}/\tilde{\delta}_{1c} \simeq (1-\alpha)^{-2}Re^{1/2}$ for the three models (NS, IBL and RNSP, in this last case the wall has been smoothed in $(x-x_g)/R_g = \pm 1$ to avoid an infinite slope, this was not the case for NS and IBL), here $\alpha = 0.75$, $Re = 500$. The upper half geometry is plotted as well (the smoothed one is not plotted). The position of the point of separation (where $\tilde{\tau} = 0$) is nearly the same in the three models.

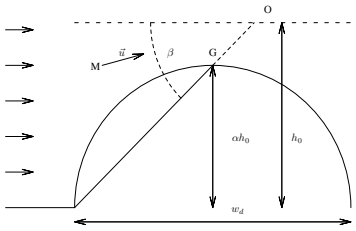

Figure 22: A very crude estimation: we replace the 2D obstacle by a triangle (!), if this obstacle is a circle the width is $w_d = 2R_0$, the height is αh_0, the channel half height is $h_0 = R_0/\alpha$. This is now the flow in a converging channel of total angle 2β, the fictitious sink is at position O, the distance (OM) from the curent point to the sink allows a simple estimation of the displacement thickness.

7 Numerical results: estimating the boundary layer thickness at the throat $\tilde{\delta}_{1c}$

The estimation of the boundary layer thickness is the key for evaluation of velocities and pressures. It is based on the fact that the stenosis is a kind of convergent channel (of half angle β with a sink at the apex). It is a classical result that there exists a selfsimilar solution (Schlichting [38] (1987)) whose boundary layer thickness divided by the distance to the sink is $0.779\beta^{1/2}Re^{1/2}$ (where Re is constructed with the half flux). Approximating the obstacle of total width w_d and of height αh_0 to a triangle, the throat is at distance $(OG) = (1-\alpha)h_0\sqrt{1+(\frac{w_d}{2\alpha h_0})^2}$ from the apex, the half angle is $\beta = \tan^{-1}(2\alpha h_0/w_d)$. In the case of a circle ($w_d = 2R_0, h_0 = R_0/\alpha$) this distance (OG) is $(1-\alpha)\sqrt{2}h_0$ and the angle is $\beta = \pi/4$, so that, in h_0 scale:

$$\tilde{\delta}_{1c} = 0.779(\pi/2)^{1/2}(1-\alpha)Re^{-1/2}. \tag{47}$$

We tested this order of magnitude (with RNSP and IBL) to be exact for a triangular glottis and to be correct for other geometries. This estimate is in fact more precise for $\alpha > 0.8$ than the one proposed by Lorthois *et al.* [**?**] in an axi-symmetrical pipe. This allows us to deduce a simplified formula for the dimentionalized pressure drop at the glottis. Knowing U_0, h_0, α, and $Re = h_0U_0/\nu$, the velocity is derived from flux conservation, and is corrected by the displacement thickness; Bernoulli law is written between the entrance and the throat, and the approximate pressure drop follows:

$$P_t - P_g \simeq -\frac{\rho U_0^2}{2}\left(\frac{1}{(1-\alpha-\tilde{\delta}_{1c})^2} - 1\right). \tag{48}$$

Furthermore we find that the ratio representing the viscous losses is nearly constant: $P_t/(P_t - P_g) \simeq K_t = 0.86$.

This estimation of the boundary layer thickness is then used to approximate the non dimensional skin friction near the throat where $H = 2.07$ and the velocity is about $(1-\alpha)^{-1}$:

$$\tilde{\tau} \simeq \frac{Hf_2(1-\alpha)^{-1}}{\tilde{\delta}_{1c}} \simeq (1-\alpha)^{-2}Re^{1/2}. \tag{49}$$

The skin friction is plotted on Figure 21, where it has been rescaled by (49). We see that this estimate may be improved but gives the good order of magnitude as the skin friction is very large. The position of the point of separation is nearly the same for the three codes.

8 Conclusion

Knowing the flux, and supposing laminar steady flow, an evaluation of boundary layer thickness issued from boundary layer theory was obtained. This evaluation leads to an estimation of the skin friction and of the pressure drop at the throat. Those estimates fit well the Interacting Boundary Layer, Reduced Navier Stokes, and Navier Stokes codes. The complete Navier Stokes resolution has the following drawbacks; first, it is far slower than the RNSP resolution, which is slower than the IBL resolution. Second, the boundary layer is so thin (as predicted by formula (47)) that one has to be very careful with the mesh in the throat. This analysis shows how usefull asymptotic theory is to analyze and understand the flow.

Part III
RNSP 2D non symmetrical

9 Introduction

Computing the flow in locally constricted pipe is important in numerous applications in biomechanics. Of course this can be achieved with accuracy through Navier-Stokes solvers. For example, in local constrictions of blood vessels (Berger and Jou [1], Siegel et al. [40]), in veins (collapsible tubes Luo & Pedley [30]) in aneurysms (or dilated tube, Budwig et al. [2]), or in the upper airway (Shome et al. [39]). Here we will focus on steady laminar flows at high Reynolds number that can be considered as bidimensional, but not symmetrical. A typical example is on figure 23. In fact we will study a model example. Our aim is to present the simplest model for steady laminar pipe flow at large Reynolds number and to observe the effect of asymmetry.

We will compare some NS (Navier Stokes) solutions to solutions of asymptotic equations because we think that they provide a better understanding of the flow structure and relevant scalings. Using asymptotic equations, computational time is drastically reduced. Therefore, parameters may be changed easily and their influence can be thoroughly investigated.

Most of such simplified previous studies considered symmetrical flows (Pelorson et al. [31], Lorthois et al. [24], Lagrée et al. [18], Lagrée et al. [**?**], de Bruin et al. [8] and Kalse et al. [15]). In [21] and [15] it was observed that integral Interacting Boundary Layer and NS give very similar results. Predictive simplified formula for values of the skin friction and for the pressure drop based on the boundary layer were presented in [24] and [18]. In [**?**], the links between the "Triple Deck" theory and Interactive Boundary Layers in internal flows is presented. Furthermore [15] proposed part of the equations for a non symmetrical channel but did not solved them. Hence, we present an asymptotic derivation of the effect of non symmetry in the framework of the Interactive Boundary Layer theory (IBL). This theory is presented in Cebeci & Cousteix [4] or Sychev et al. [48], as not complete in the asymptotical framework. But, they point out that numerous results of calculations for different flows showed good agreement with experimental data in the description of flow separation in aerodynamics. In Veldman [51] the IBL and its links with the "Triple Deck" theory in open flows is explained. Some industrial examples comparing IBL and experiments are presented too.

Mainly, the descriptions of IBL use the length of the bump as fundamen-

tal scale (say L). The Reynolds number is then constructed with this length ($R_L = U_0 L/\nu$, here we are in a 2D channel, h_0 is the distance between the two plates, and $U_0 h_0$ is the flux). The boundary layer is then scaled by $LR_L^{-1/2}$, the displacement thickness is about $1.7LR_L^{-1/2}$. This length L must be smaller that the length of entry (say L_e) which is such that the two boundary layers merge between the plates: $L_e R_{L_e}^{-1/2} = h_0$. This length is $L_e = h_0(U_0 h_0/\nu)$. The idea of the IBL theory is to couple the ideal fluid flowing in the core to variations of the displacement thickness of the boundary layer. For example, before the constriction, where the walls are flats, it means that the ideal fluid in the pipe experiments no more the section h_0 but a smaller section reduced by twice $1.7LR_L^{-1/2}$. So the flow is accelerated. In "classical boundary layer theory" it is impossible: the Reynolds is infinite ($R_L^{-1/2} = 0$). The entry length is reject at infinity. This boundary layer effect is an order two effect (Van Dyke [50]), the velocity remains U_0. But in "IBL theory" this is possible. It means that $R_L^{-1/2}$ is small but not so much. Hence, effect of second order and first order are mixed: the boundary layer retroacts on the ideal fluid. This was the paradox of IBL.

But, recently, Dechaume et al. [9] (and Cousteix and Mauss [5] and [6]) established on rational basis the IBL equations. They break the paradox. They use a "modified Van-Dyke" principle and "successive complementary expansion method". The existence of a small parameter in the equation is then no more a problem. The link with "Triple Deck" theory is done as well. They show that with this technique the IBL equations are fully justified.

Here, as we are in pipe, we prefer to use h_0 to construct the Reynolds ($Re = U_0 h_0/\nu$) and to scale the boundary layer. So to have a small boundary layer as just mentioned, we have to be near the entrance of the pipe at a distance smaller than $L_e = h_0(U_0 h_0/\nu)$ (so that we are before the merging of the boundary layers). Compared to the previous approach where we gave L, it is just a change of scale of the boundary layer equations. This length must be larger than the distance between the plates in order to do the expansion in the ideal fluid. But we will observe that the system is very robust and may be used even if the width of the bump is h_0. One reason of this robustness is that the flow is accelerated, so that the boundary layer is thinner. The other one belongs to magic of asymptotic expansion which give often good results even if the small parameter is not so small (Van Dyke [50]).

First we present the problem and the basic scales for the NS problem. Then we introduce a simplified set of equations: Reduced Navier Stokes. The integral IBL system is introduced thereafter. A comparison between the three models shows that the integral IBL catches most of flow features

(with a very short computational time, about 500 times less).

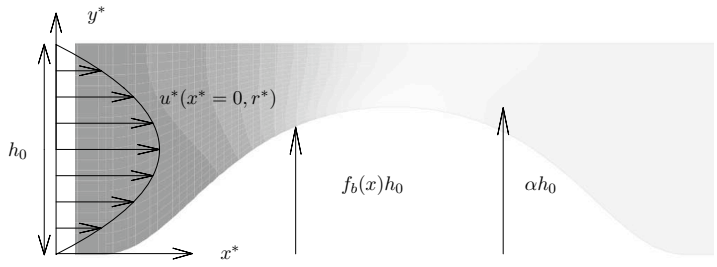

Figure 23: A zoom of the channel with its stenose. The constriction is a smoothed ellipsis (the lower wall is f_b, the upper is here flat, $f_h = 0$). The transverse scale is adimensionalised by the unperturbed channel width h_0. Here, the entry profile is a Poiseuille profile ($u = U_{Pois} = y(1-y)$ and $v = 0$), but any other is possible. The NS computational domain is larger to avoid entrance and output effects, iso pressure (gray scale) and the mesh (white grid) are plotted.

10 Equations

10.1 Navier Stokes

We solve the Newtonian steady laminar incompressible bidimensional Navier Stokes equations with the numerical code Castem 2000 [29]. The geometry consists in a straight channel with a bump on one wall (figure 23), we used the channel height h_0 to nondimensionalise the scales of x^* and y^*. A Poiseuille velocity (of total flux $U_0 h_0$ equal to 1 in non dimensional scales) is imposed at the entrance, a zero stress is imposed at exit. The exit and the entrance are far enough from the stenosis to avoid their influences. We present (on fig. 1 to 5) only results for $Re = 500$ ($Re = U_0 h_0/\nu$). Increasing the Reynolds increases the number of points and the computational time. It creates problems at the output where the jet may oscillate. But we do not focus here on the NS problem.

10.2 Reduced Navier Stokes

We now present two simplifications of the NS equations issued from boundary layer theory (Schlichting [38], Sychev et al. [48], Rubin and Tannehill [35]). The first simplification consists in neglecting the transverse variation of pressure. This leads to a system we call RNSP (Reduced Navier Stokes/ Prandtl) because this is a reduced system obtained from Navier Stokes and because this is in fact the Prandtl partial differential equations (with different boundary condition than in the classical boundary layer theory). It has been shown that this system is a good approximation of NS in symmetrical stenoses (Lagrée et al. [18]) and that its axisymmetrical version (Lagrée & Lorthois [22]) includes most of IBL/ Triple Deck/ Double Deck asymptotical régimes. These equations are obtained from NS by supposing that the transverse scale is smaller than the longitudinal one and that the Reynolds number is large. To settle the equations, u^* is scaled by U_0, v^* by U_0/Re, x^* by $h_0 Re$, y^* by h_0 and p^* by ρU_0^2. The flow is supposed quasistatic: Strouhal number is low, in fact the spatial acceleration is large. The system is:

$$\frac{\partial}{\partial x}u + \frac{\partial}{\partial y}v = 0, \qquad u\frac{\partial}{\partial x}u + v\frac{\partial}{\partial y}u = -\frac{\partial}{\partial x}p + \frac{\partial^2}{\partial y^2}u, \qquad 0 = -\frac{\partial}{\partial y}p. \quad (50)$$

The boundary conditions are no slip $u(x, y = f_b(x)) = 0$, $v(x, y = f_b(x)) = 0$ at the lower wall defined by $f_b(x)$ (whose dimension is h_0) and at the upper wall $u(x, y = 1 - f_h(x)) = v(x, y = 1 - f_h(x)) = 0$. At the entrance, pressure is zero, the first velocity profile is given (for example a flat profile $u = 1$, $v = 0$, or Poiseuille).

We note the invariance by Prandtl transform ($y^p = y - f_b(x)$) that allows to solve the problem from $y^p = 0$ to $y^p = 1 - f_h(x) - f_b(x)$.

We note that there are two transverse boundary conditions ($u(x, y = f_b(x)) = 0$ and $u(x, y = 1 - f_h(x))$ but there is no outflow boundary condition (only $u = 1$ is given at the entrance). This is because the system is parabolic in x ($u\partial_x u \simeq \partial_y^2 u$). The Navier Stokes equations must have an output condition, which is not the case here.

10.3 IBL

10.3.1 Ideal Fluid

Previous studies used mainly a symmetrical approximation, so that ideal fluid pressure or ideal fluid velocity was a function of the longitudinal vari-

able alone. We want to introduce a small effect of transverse variation of pressure. Then we will couple the ideal fluid with the two boundary layers.

We solve linearized Euler equations in a channel with a slowly varying indentation with ($\xi = \varepsilon x^*/h_0$, $y = y^*/h_0$). Thereafter ξ will be identified with x. In practice, we will discuss the flow with a flat upper wall ($y_h = 1$ or $f_h = 0$), with an indentation at the lower wall ($y_b = f_b$). The maximum value of f_b is α the degree of stenosis, the indentation may be severe, it means that α may be close to 1. Expanding as:

$$u = U_0(\xi) + \varepsilon u_1(\xi, y) + \varepsilon^2 u_2(\xi, y) + ..., \tag{51}$$

$$v = \varepsilon v_1(\xi, y) + \varepsilon^3 v_3(\xi, y) + ..., \tag{52}$$

$$p = p_0(\xi) + \varepsilon p_1(\xi, y) + \varepsilon^2 p_2(\xi, y) + ..., \tag{53}$$

so that Euler system (we note that the perturbations u_1 and p_1 are zero) is at order 0 and 1:

$$U_0 \frac{\partial U_0}{\partial \xi} = -\frac{\partial p_0}{\partial \xi}, \tag{54}$$

and

$$\varepsilon \frac{\partial U_0}{\partial \xi} + \varepsilon \frac{\partial v_1}{\partial y} = 0. \tag{55}$$

(The flow was supposed irrotational $\partial_y U_0 - O(\varepsilon^2) = 0$). Writing the no slip condition on the upper and lower walls (resp. y_h and y_b):

$$v_1(\xi, y_b = f_h) = U_0 \frac{\partial f_b}{\partial \xi}, \qquad v_1(\xi, y_h = 1 - f_h) = -U_0 \frac{\partial f_h}{\partial \xi},$$

we integrate twice the continuity equation (55) to obtain the classical expression of U_0 and by the momentum equation (54) we obtain P_0:

$$U_0(\xi) = \frac{1}{1 - f_b(\xi) - f_h(\xi)}, \qquad P_0(x) = \frac{1}{2} - \frac{1}{2}\Big(\frac{1}{1 - f_b(\xi) - f_h(\xi)}\Big)^2. \tag{56}$$

The expression for transverse velocity follows:

$$v_1(\xi, y) = U_0 \frac{\partial f_b}{\partial \xi} + \frac{y - f_b}{1 - f_h - f_b}(-U_0 \frac{\partial f_b}{\partial \xi} - U_0 \frac{\partial f_h}{\partial \xi}) \tag{57}$$

The next order is:

$$\varepsilon^2 U_0 \frac{\partial v_1}{\partial \xi} = -\varepsilon^2 \frac{\partial p_2}{\partial y}, \tag{58}$$

$$\varepsilon^3 \frac{\partial U_0 u_2}{\partial \xi} = -\varepsilon^3 \frac{\partial p_2}{\partial \xi}, \tag{59}$$

$$\varepsilon^3 \frac{\partial u_2}{\partial \xi} + \varepsilon^3 \frac{\partial v_3}{\partial y} = 0. \tag{60}$$

From the integration by y of the incompressibility at order 0 and 2, we obtain that $\partial_\xi(\int_{y_b}^{y_h}(U_0 + \varepsilon^2 u_2)dy) = 0$, once developed using (57) and from Euler equation (59) we then obtain $\int_{y_b}^{y_h} p_2 dy = 0$. After some algebra, from (58) and (57), we find the pressure value at order 2 on the lower wall:

$$\begin{aligned} p_2(\xi, f_b) &= \frac{-4\, f_b'(\xi)^2 - 2\, f_b'(\xi)\, f_h'(\xi) + 2\, f_h'(\xi)^2}{6\, (-1 + f_b(\xi) + f_h(\xi))} + \\ &+ \frac{(-1 + f_b(\xi) + f_h(\xi))\, (2\, f_b''(\xi) - f_h''(\xi))}{6\, (-1 + f_b(\xi) + f_h(\xi))}, \end{aligned} \tag{61}$$

and the pressure value at order 2 at the upper wall:

$$\begin{aligned} p_2(\xi, 1 - f_h) &= \frac{-\left(-2\, f_b'(\xi)^2 + 2\, f_b'(\xi)\, f_h'(\xi) + 4\, f_h'(\xi)^2\right)}{6\, (-1 + f_b(\xi) + f_h(\xi))} + \\ &+ \frac{(-1 + f_b(\xi) + f_h(\xi))\, (f_b''(\xi) - 2\, f_h''(\xi))}{6\, (-1 + f_b(\xi) + f_h(\xi))}. \end{aligned} \tag{62}$$

We define the total transverse pressure drop as $\varepsilon^2(p_2(\xi, y_h) - p_2(\xi, y_b))$, which is a bit more simple:

$$\varepsilon^2(p_2(\xi, y_h) - p_2(\xi, y_b)) = \varepsilon^2\Big(\frac{(f_h'(\xi)^2 - f_b'(\xi)^2)}{1 - f_b(\xi) - f_h(\xi)} + \frac{(f_h''(\xi) - f_b''(\xi))}{2}\Big). \tag{63}$$

Of course, a symmetrical channel ($f_b = f_h$) gives $\Delta P_0 = 0$, in practice we will use $f_h = 0$. We note that Kalse *et al.* [15] derived with more severe approximations this same pressure drop (but not (61) nor (62)). Here the result comes only from the hypothesis.

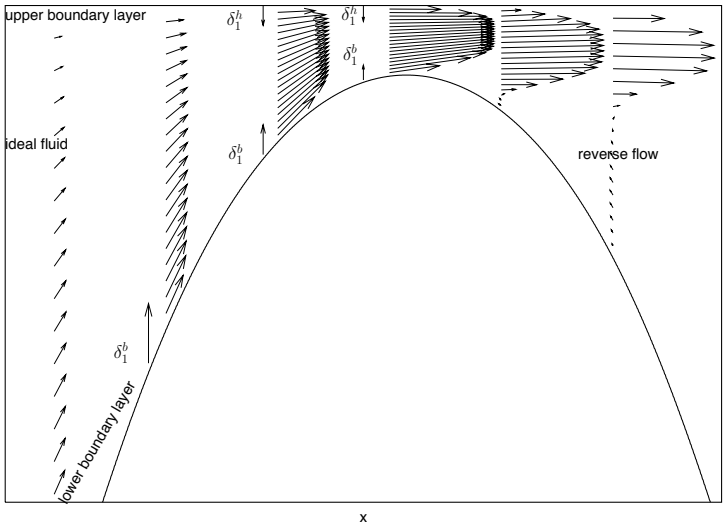

Figure 24: A larger zoom of the channel (here a RNSP computation at $Re = 500$) with the stenose and the upper flat wall. The two upper and lower boundary layers and the ideal fluid appear from the computation. The interaction between the ideal fluid and the boundary layers is the core of the Interactive Boundary Layer theory.

10.3.2 Boundary layer

Up to now in this section, we supposed that the fluid was ideal. Here we introduce the Boundary Layer equations which may be deduced from Navier Stokes supposing that the Reynolds number is large and that viscous effects are restricted to two thin layers near the walls (see figure 24). We simplify much more the boundary layer in using the integral Kármán equation ([38], [12]). We define δ_1^b and δ_1^h the displacement thicknesses at the lower and the upper walls. The choice of the scalling comes here from the RNSP case, x is scaled by $h_0 Re$ and $\delta_1^{b,h}$ by h_0, in fact the boundary layer will be small at those scales (see Lagrée & Lorthois [22]). This slow variation in x allows to identify Re^{-1} and ε. So, this gives the following system where the ideal fluid (computed in the preceding section) promotes the boundary layer. We have two boundary layers, one at the top:

$$\frac{d}{dx}(\frac{\delta_1^h}{H}) + \frac{\delta_1^h}{u_e^h}(1+\frac{2}{H})\frac{du_e^h}{dx} = \frac{f_2 H}{\delta_1^h u_e^h}, \qquad \delta_1^h = F(u_e^h), \tag{64}$$

and another at the bottom:

$$\frac{d}{dx}(\frac{\delta_1^b}{H}) + \frac{\delta_1^b}{u_e^b}(1+\frac{2}{H})\frac{du_e^b}{dx} = \frac{f_2 H}{\delta_1^b u_e^b}, \qquad \delta_1^b = F(u_e^b). \tag{65}$$

Initial condition is for example $\delta_1^{h,b}(0) = 0$ and $u_e^{h,b}(0) = 1$. In the classical approach, δ_1 is obtained through the knowledge of u_e, which we write formaly $\delta_1^{b,h} = F(u_e^{b,h})$. To solve these boundary layer equations, a closure relationship linking H and f_2 to the velocity and the displacement thickness is needed. This is of course a strong hypothesis. Defining $\Lambda_1 = \delta_1^2 \frac{du_e}{dx}$, (of course it is δ_1^b, u_e^b or δ_1^h, u_e^h) the system is closed from the resolution of the Falkner Skan system as follows:

$$H = \left\{ \begin{array}{ll} 2.5905 e^{-0.37098\Lambda_1} & \text{if } \Lambda_1 < 0.6 \\ 2.074 & \text{if } \Lambda_1 > 0.6 \end{array} \right\}, \qquad f_2 = 1.05(-H^{-1} + 4H^{-2}).$$

It means that we suppose that each profile remains a Falkner Skan one in the boundary layer.

This closure allows flow separation for decelerated flows, we will see in the next section that one has to solve these equations (64 and 65) in an "inverse way" ($u_e^{b,h} = F^{-1}(\delta_1^{b,h})$) to compute flow separation.

Those simplifications are in the spirit of Lorthois *et al.* [**?**], but here in 2D. Recently, Kalse *et al.* [15] used nearly the same modelisation.

10.3.3 Integral IBL

The Integral Boundary Layer equations (IBL) suppose that the wall is no more at the bottom $y_b = f_b$ and at the channel height $y_h = 1 - f_h$ but it is changed by the amount of the displacement boundary layer thickness δ_1^h at the upper wall and δ_1^b at the lower wall. That is why we scaled $\delta_1^{b,h}$ by h_0 and why we identified ε to be Re^{-1} and $x = \xi$.

This gives a coupled system where the ideal fluid promotes the boundary layer: (64) and (65) that, in growing, retroacts (with the help of the concept of displacement thickness) on the ideal fluid through the flux conservation. The mean velocity (56) is no more $(1 - f_b(x) - f_h(x))^{-1}$ but is now $(1 - (f_b(x) + \delta_1^b(x)) - (f_h(x) + \delta_1^h(x)))^{-1}$. The ideal fluid relation is now:

$$P_0(x) = \frac{1}{2} - \frac{1}{2}\Big(\frac{1}{1 - (f_b(x) + \delta_1^b(x)) - (f_h(x) + \delta_1^h(x))}\Big)^2. \qquad (66)$$

Using IBL idea (where first and second order are mixed), we say that the pressure are in fact $p^b = P_0(x) + \varepsilon^2 p_b(x, y_b = 1 - (f_b + \delta_1^b))$ and $p^h = P_0(x) + \varepsilon^2 p_h(x, y_h = f_h + \delta_1^h)$. The pressure at the bottom $(p^b(x, y_b = f_b + \delta_1^b))$ is (61) with f_b changed by $f_b + \delta_1^b$; the same for $p^h(x, y_h = 1 - (f_h + \delta_1^h))$ which is (62) with f_h changed by $f_h + \delta_1^h$. As the expressions for $p^b(x, y_b = f_h + \delta_1^h)$ and $p^h(x, y_h = f_h + \delta_1^h)$ are a bit complicated, we just write their difference $p^h - p^b = \Delta P_0$:

$$\Delta P_0 = \varepsilon^2\Big(\frac{\left((f_h' + \delta_1'^h)^2 - (f_b' + \delta_1'^b)^2\right)}{1 - (f_b + \delta_1^b) - (f_h + \delta_1^h)} + \frac{\left(f_h'' + \delta_1''^h - f_b'' - \delta_1''^b\right)}{2}\Big). \qquad (67)$$

Note that we recover a result that looks like Smith [42] (or Sobey [46]) result in pipe flow, the transversal perturbation of pressure in a perturbed Poiseuille flow is $p_h - p_b = A''/30$ where $-A$ is a displacement of the stream lines as $\delta_1^b - \delta_1^h$ is. Of course the two configurations are very different.
We note that this coupling relation produces upstream influence, it means that before the bump, the flow "knows" that it is comming. This creates solutions in e^{kx} with $k > 0$, we see it on the numerical solutions.

10.3.4 Numerical resolution of the Integral IBL

We solve the interactive system by a semi inverse method (Le Balleur [25]). This means that the boundary layer is solved in an inverse way (the displacement thickness is imposed and the velocity is a result of the computation). This inverse way allows to compute flow separation (the direct way would

lead to a singularity at separation). The ideal fluid is computed in "direct way" from the geometry changed by the amount of the boundary layer displacement thickness.

At iteration n, we have a set of two displacement boundary layer thickness $(\delta_1^b)^n$ and $(\delta_1^h)^n$. They give, by solving in an inverse way (64) and (65), two associated boundary layer velocities: $(u_e^h)^n = F^{-1}((\delta_1^h)^n)$ and $(u_e^b)^n = F^{-1}((\delta_1^b)^n)$.

The two corresponding pressures in the boundary layers $(p_e^h)^n$ and $(p_e^b)^n$ are computed from these velocities, i.e. Bernoulli:

$$(p_e^{(b,h)})^n = \frac{1}{2}(1 - ((u_e^{(b,h)})^n)^2). \tag{68}$$

From the expressions of $p^h(x, y_h = f_b + \delta_1^b))$ and $p_b(x, y_b = f_b + \delta_1^b))$ (defined before equation 67), the ideal fluid pressures are computed. A new boundary condition associated to the second derivative must be used. At the output $\frac{\partial p^h}{\partial x} = 0$ and $\frac{\partial p^b}{\partial x} = 0$ are imposed.

The semi inverse relaxation is done as follows (figure 25):

$$(\delta_1^h)^{n+1} = (\delta_1^h)^n + \lambda((p^h)^n - (p_e^h)^n) \tag{69}$$

$$(\delta_1^b)^{n+1} = (\delta_1^b)^n + \lambda((p^b)^n - (p_e^b)^n). \tag{70}$$

The relaxation parameter λ is chosen by trial and error in order to obtain convergence. In order to obtain estimate of λ the theory proposed by Le Balleur [25] is relevant.

11 Some numerical comparisons

We compare then the NS results to the RNSP and IBL results. We suppose that the upper wall is flat $f_h = 0$, and that the lower wall is a given function of x^*, for example the following function is close to half a circle:

$$\zeta = \frac{x^* - x_c^*}{4\alpha h_0/3}, \qquad f_b(\zeta) = 1 - \frac{\zeta^2}{2} - \frac{\zeta^4}{8} - \frac{\zeta^6}{16} + \frac{1445\zeta^8}{13122} - \frac{1385\zeta^{10}}{59049},$$

which is nearly $\sqrt{1-\zeta^2}$ around $\zeta = 0$ up to order ζ^8. Notice that on every figure we used the physical longitudinal scale (h_0) to plot the curves; numerically in (50) and (64, 65), the width of the bump is of order $(1/Re)$ in our scales.

The first curves show the pressure (Fig. 26) and the skin friction (Fig 27) computed by RNSP and NS. We see that the pressure $p(x)$ from RNSP

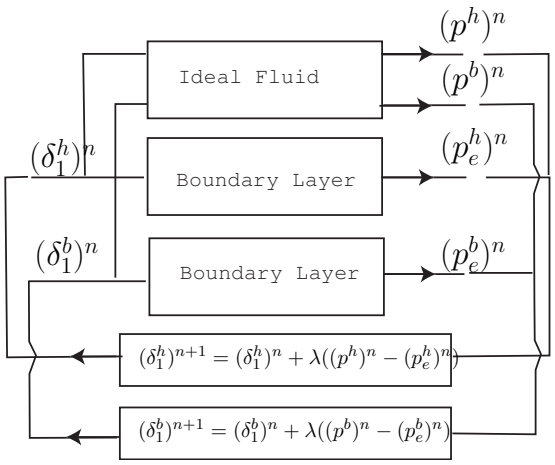

Figure 25: A chart of the iterative "semi inverse" interaction: the two boundary layers are solved in an inverse way. The correction of boundary layer thickness is proportional to the difference of pressure.

is an approximation of the mean NS pressure. The NS pressure displays a larger drop just after the throat on the curved wall and a smaller pressure drop on the flat wall. The recompression is over predicted by RNSP. In the symmetrical cases ([22]) the difference was smaller.

The RNSP skin friction overall distribution looks like the NS one. There is a kink in the skin friction at the flat wall which does not exist in NS because of the smoother pressure gradient on the flat wall.

The next curves show the pressure (Fig. 28) and the skin friction (Fig. 29) computed by integral IBL and NS. They show "upstream influence", the upstream part of the flow is influenced by the downstream part. On the pressure curve, before the throat, the upstream influence of the bump is to produce an over pressure drop on the curved wall. This upstream influence comes from the order two derivative in the transverse pressure relation (Eq 67), it has an exponential behavior (e^{kx} with $k > 0$). This influence is responsible for the incipient separation before the bump, increasing α leads to flow separation before the bump. This upstream influence is due to the curvature of the stream line. It does not exist in the symmetrical case.

The integral IBL skin friction looks like the NS one, but it is overestimated by the IBL (results from integral IBL will never be perfect because

there is a strong closure hypothesis). The integral IBL well predicts the position of the point of separation but overpredicts the negative skin friction. The incipient separation before the bump is well predicted and is related to the upstream influence.

The displacement functions δ_1^b and δ_1^h (IBL flat) are plotted on figure (Fig. 30). A large value of the displacement thickness is associated to a deceleration of the flow and eventually to boundary layer separation. A thin value is associated to the large acceleration at the throat. The difference of pressure $p^h - p^b$ is plotted too. As this difference of pressure has scale Re^{-2} the effect of asymmetry becomes smaller with larger Re.

The integral IBL gives good trends in the influence of asymmetry, its main advantage is that it is a extremely quick method compared to full Navier Stokes which is time and memory consuming. For example, using a Linux x86 workstation at 3.0 GHz we may roughly compare the three methods. Navier Stokes solver CASTEM takes about 15 minutes to compute the flow (200 times 16 nodes) for a maximal error of 10^{-5} between two iterations. RNSP solver takes 2 seconds to compute the flow (on a very fine mesh 3000 times 1000). Finally, the integral IBL solves a symmetrical case in less than 0.5 second; it needs 2 more seconds to obtain a maximal error of 10^{-5} between two iterations in the non symmetrical case (in about 800 iterations). Those figure are indicative, faster NS solvers may exist, and our code is not optimised.

Increasing the Reynolds number will disadvantage the Navier Stokes computation: the IBL remains always precise, but the NS mesh has to be refined.

12 Conclusion

We have presented here a simplified model issued from asymptotic analysis. The expressions of the pressure at the upper and lower wall were presented. The effect of asymmetry is an order two effect. The integral Boundary Layer equations are solved together with the ideal fluid equations thanks to Interactive Boundary Layer Theory.

A symmetrical pipe has no upstream influence, it means that changing the downstream conditions does not change the flow upstream. This is broken by the asymmetry. Concerning the pressure, the effect of asymmetry is to increase the pressure drop at the curved bottom wall and to lower the pressure at the flat upper wall. The smallest pressure is on the curved wall, the minimum pressure on the bottom wall is more upstream that the pressure

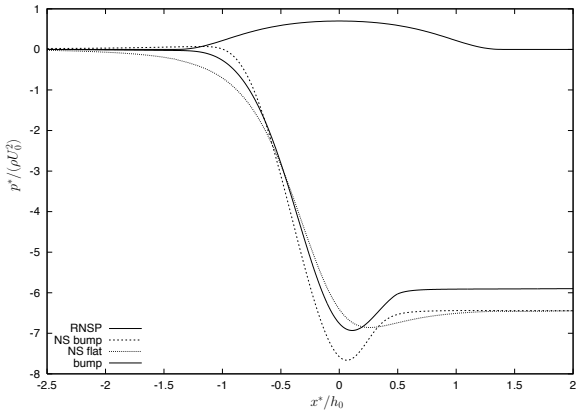

Figure 26: Comparison of RNSP and NS pressures, RNSP solution is an approximation of the two NS pressures. The geometry is plotted as well.

minimum on the top wall. The two minima are after the throat. A massive separation appears after the throat on the curved wall, a small separation appears before the throat on the curved wall, no separation occurs at the flat wall. The effect of downstream on upstream that is not present in the RNSP theory is a pure effect of the wall and displacement curvature. This effect creates an increase of pressure on the lower wall which is responsible for the upstream flow separation.

Solving the equations of IBL theory is very fast (from factor 2000 in the symmetrical case to a factor 500 in the non-symmetrical case), so we plan to use it in biomecanical fluid structure interactions such like the Obstructive Sleep Apnea syndrome.

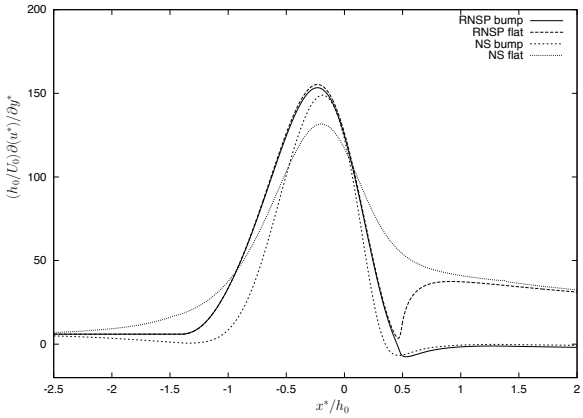

Figure 27: Comparison of RNSP and NS wall shear stress. The flat wall shear stress is over predicted by RNSP at the maximum, but in the wake ($x^*/h_0 > 1$) it is better.

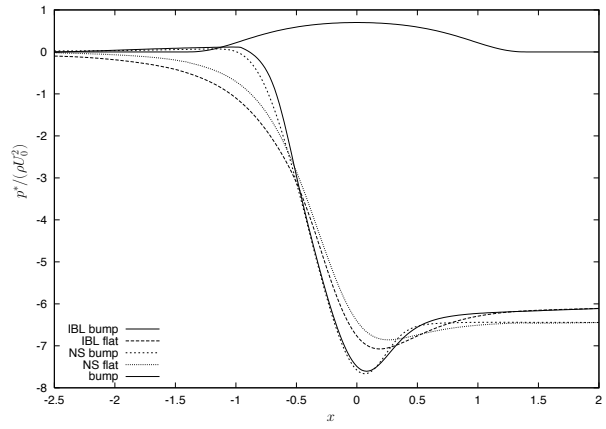

Figure 28: Comparison of integral IBL and NS pressures. The IBL approach well predicts the over pressure on the flat wall and the positions of the minima of of the pressures after the throat.

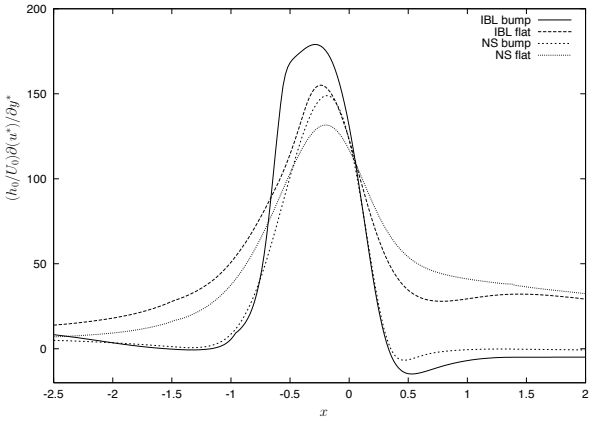

Figure 29: Skin friction, comparison of integral IBL and NS. The integral IBL over predicts the maximum of skin friction but well predicts the position of the point of separation. The incipient separation before the bump is well predicted.

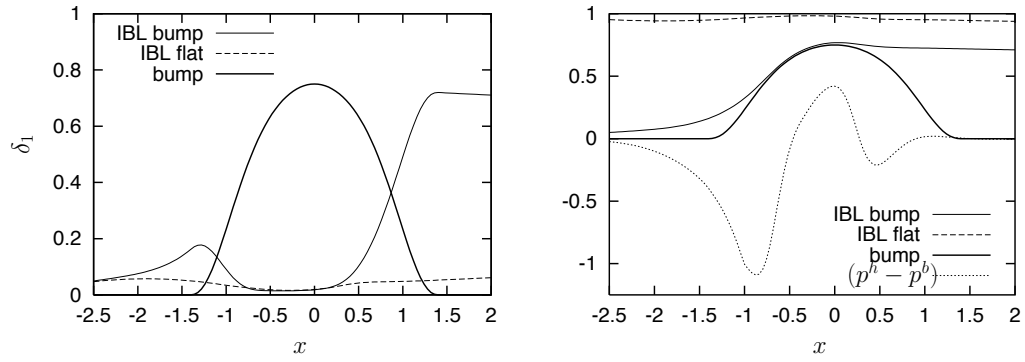

Figure 30: Left: the displacement functions δ_1^b (IBL bump) and δ_1^h (IBL flat). A large value of δ_1 is associated to boundary layer separation. A thin value is associated to the large acceleration at the throat. Right: the difference of pressure $p^h - p^b$ is plotted, the "final effective" channel is plotted: $1 - \delta_1^h$ and $f_b + \delta_1^b$; the jet due to separation is visible.

References

[1] Berger S. A. & Jou L-D. (2000): "Flows in stenotic vessels", Annu. Rev. Fluid Mech. 2000. 32, pp. 347-382.

[2] Budwig R., Elger D., Hooper H. & Slippy J. (1998): "Steady flow in abdominal aortic aneurysm models", J. Biomech. Eng., vol 115, nov., pp. 419- 423.

[3] Bluestein D., Niu L., Schoephoerster R.T. & Dewanjee M.K. (1996): "Steady flow in an aneurysm model: correlation between fluid dynamics and blood platelet deposition", J. Biomech. Eng., vol 118, aug., pp 280-286.

[4] Cebeci T. & Cousteix J. (1999): "Modeling and computation of boundary layer flows", Springer Verlag.

[5] Cousteix J., & Mauss J. (2004): "Approximations of the Navier-Stokes equations for high Reynolds number flows past a solid wall" Journal of Computational and Applied Mathematics 166(1): 101-122, 2004.

[6] Cousteix J., & Mauss J. (2006): "Analyse asymptotique et couche limite", Mathématiques et Applications, Vol. 56 2006, XII, 396 p.

[7] Davis R.T., Barnet M. & Rakich J. V. (1986): "The calculation of supersonic viscous flows using the parabolized Navier-Stokes equations", Computers Fluids Vol 14, No 3, pp 197- 224.

[8] de Bruin B., Lagrée P-Y, Lorthois S., Vilain C., & Veldman A.E.P. (2001): "Comparison of Navier-Stokes and Reduced Navier-Stokes unsteady computation in a stenosis", Archives Physiol. Biochem. V109, 09/2001 p79.

[9] A. Dechaume, J. Cousteix and J. Mauss (2005): "An interactive boundary layer model compared to the triple deck theory", European Journal of Mechanics - B/Fluids, Volume 24, Issue 4, July-August, pp. 439-447.

[10] Fletcher C.A.J. (1991): "Computational techniques for fluid dynamics, vol II", Springer Verlag.

[11] Gajjar J. & Smith F.T. (1983): "On hypersonic self induced separation, hydraulic jumps and boundary layer with algebraic growth", Mathematika, 30, pp. 77-93.

[12] Gersten, K. and Hervig, H. (1992): "Strömungsmechanik : Grundlagen der Impuls-Wärme-und Stoffübertragung aus asymptotischer Sicht", Vieweg, Wiesbaden.

[13] P.M. Gresho (1991): "Incompressible fluid dynamics: some fundamental formulation issues", Annu. Rev. Fluid Mech. 23, pp 413-453.

[14] Huang, H., Modi, V. J., & Seymour, B. R., (1995): FluidMechanics of StenosedArteries, Int. J. Eng. Sci., 33, pp. 815828.

[15] S. G. C. Kalse, H. Bijl, and B. W. van Oudheusden (2003): "One-Dimensional Viscous-Inviscid Strong Interaction Model for Flow in Indented Channels With Separation and Reattachment", Journal of Biomechanical Engineering, Volume 125, Issue 3, pp. 355-362.

[16] Lagrée P.-Y. (1998): "Écoulement dans un anévrisme: comparaison de différentes méthodes de type couche limite", Archives Physiol. Biochem. Vol 106 supp B, septemb 98, p 42.

[17] Lagrée P.-Y. (2000): "An inverse technique to deduce the elasticity of a large artery ", European Physical Journal, Applied Physics 9, pp. 153-163

[18] P.-Y. Lagrée, E. Berger, M. Deverge, C. Vilain & A. Hirschberg (2005): "Characterization of the pressure drop in a 2D symmetrical pipe: some asymptotical, numerical and experimental comparisons", ZAMM: Z. Angew. Math. Mech. 85, No. 2, pp. 141-146.

[19] P.-Y. Lagre, A. Van Hirtum & X. Pelorson (2007): "Asymmetrical effects in a 2D stenosis". European Journal of Mechanics - B/Fluids, Volume 26, Issue 1, January-February 2007, Pages 83-92

[20] Lagrée P.-Y. & Lorthois S. (1999): "Interacting Boundary layer flow in a stenosis". Archives Physiol. Biochem. Vol 107 sept 99, p 51.

[21] Lagrée P.-Y., Berger E., Deverge M., Vilain C. & Hirschberg A. (2005): "Characterization of the pressure drop in a 2D symmetrical pipe: some asymptotical, numerical and experimental comparisons", ZAMM, 5, No. 2, pp. 141-146.

[22] P.-Y. Lagrée & Sylvie Lorthois (2005),"The RNS/Prandtl equations and their link with other asymptotic descriptions: application to the wall shear stress scaling in a constricted pipe", International Journal of Engineering Sciences, Vol 43/3-4 pp 352-378

[23] Lorthois S. & Lagrée P.-Y. (2000): "Écoulement dans un convergent axisymétrique: calcul de la contrainte de cisaillement pariétal maximale/ Flow in a axisymmetric convergent: evaluation of maximum wall shear stress", C. R. Acad. Sci. Paris, t328, Série II b, p33-40.

[24] Lorthois S., Lagrée P.-Y., Marc-Vergnes J.-P., & Cassot. F. (2000): "Maximal wall shear stress in arterial stenoses: Application to the internal carotid arteries", Journal of Biomechanical Egineering, Volume 122, Issue 6, pp. 661-666.

[25] Le Balleur, J.C. (1978): "Couplage visqueux non-visqueux : Méthode numérique et applications aux écoulements bidimensionnels transsoniques et supersoniques", La recherche Aérospatiale.1978-2, 67-76, Eng Trans ESA TT-496.

[26] Maslov A. A., Mironov S. G., Poplavskaya T. V. , Shiplyuk A. N. & Vetlutsky V. N. (1999): "Viscous shock layer on a plate in hypersonic flow", Eur. J. Mech. B/Fluids, vol 18, No 2, pp 213-226.

[27] Morgan P.E., Rubin S.G. & Khosla P.K. (1999): "Application of the reduced Navier-Stokes methodology to flow stability of Falkner-Skan class flows", Computers Fluids 28, pp 307-321.

[28] Neiland V. Ya (1969): "Propagation of perturbation upstream with interaction between a hypersonic flow and a boundary layer", Mekh. Zhid. Gaz., Vol. 4, pp. 53-57.

[29] H. Paillère & F. Dabbene (1994): "Initiation à la simulation numérique en mécanique des fluides à l'aide de Castem 2000", éditions ENSTA, Paris, 328p.

[30] Pedley T.J. (1980): "The fluid mechanics of large blood vessels", Cambridge University press.

[31] Pelorson X., Hirschberg A., van Hassel R.R. , Wijnands, A.P.J., Auregan Y., (1994): ''Theoretical and experimental study of quasisteady flow separation within the glottis during phonation", J. Acoust. Soc. Am 96, p. 3416-3431.

[32] Peyret R. & Taylor T.D. (1983): "Computational Fluid Dynamic" Springer Verlag.

[33] Reyhner T. A. & Flügge Lotz (1968): The interaction of a shockwave with a laminar boundary layer", Int. Non-Linear Mech., 3, pp173-199.

[34] Ruban A.I. & Timoshin S.N. (1986): "Propagation of perturbations in the boundary layer on the walls of a flat channel", MZG 2, pp. 74-79.

[35] S G Rubin, J C Tannehill (1992): "Parabolized/Reduced Navier-Stokes Computational Techniques", Annual Review of Fluid Mechanics, January 1992, Vol. 24, Pages 117-144

[36] Rubin S.G. & Himansu A. (1989): "Convergence properties of high Reynolds number separated flow calculations", Int J. Num Meth Fluids vol 9 1395-1411.

[37] Saintlos S. & Mauss J. (1996): "asymptotic modelling for separating boundary layers in a channel", Int. J. Engng. Sci.,Vol 34, No 2, pp201-211.

[38] Schlichting H. (1987): "Boundary layer theory" 7th ed Mc Graw Hill.

[39] B. Shome, L. Wang, M. Santare, A. Prasad, A. Szeri, & D. Roberts (1998): "Modeling of Airflow in the Pharynx With Application to Sleep Apnea", vol 120, 3, pp. 416- 422.

[40] Siegel J.M, Markou C.P., Ku D.N. & Hanson, S.R (1994): "A scaling law for wall shear stress through an arterial stenosis", ASME J. Biomeh. Eng. 116, 446- 451.

[41] Smith F. T. (1976): "Flow through constricted or dilated pipes and channels", part 1 and 2, Q. J. Mech. Appl. Math. vol 29, pp 343- 364 & 365- 376.

[42] F.T. Smith (1976) "Flow through constricted or dilated pipes and channels Parts 1 and 2", Q. J. Mech. Appl. Math. (29) 232- 253 and 254-265

[43] Smith F. T.(1982): "On the high Reynolds number theory of laminar flows", IMA J. Appl. Math. 28 207-81.

[44] Stewartson K. & Williams P.G. (1969): "Self - induced separation",Proc. Roy. Soc. London, A 312, pp 181-206.

[45] Stewartson K. (1974): "Multistructured boundary layer on flat plates and related bodies" Advances Appl. Mech. 14 p145-239.

[46] I.J. Sobey (2000): "Introduction to interactive boundary layer theory", Oxford University Press, applied and engineering mathematics, 256 p.

[47] Stroud J.S., Berger S. A. & Saloner D. (2000): "Influence of stenosis morphology on flow through severely stenotic vessels: implications for plaque rupture", J. Biomech. 33 (2000) pp. 443-455.

[48] Sychev V. V. , Ruban A. I. , Sychev V. V. & Korolev G. L. (1998): "Asymptotic theory of separated flows", Cambridge University Press.

[49] Tannehil J. C., Anderson D. A. & Plettcher R. H. (1997): 'Computational fluid mechanics and heat transfer", Taylor & Francis.

[50] Van Dyke M. (1975): "Perturbation Methods in Fluid Mechanics" Parabolic Press.

[51] A.E.P. Veldman (2001): "Matched asymptotic expansions and the numerical treatment of viscous-inviscid interaction", Journal of Engineering Mathematics, Volume 39, Issue 1, March, pp. 189 - 206

The web page of this text is:
`http://www.lmm.jussieu.fr/~lagree/COURS/CISM/`

The last version of this file is on:
`http://www.lmm.jussieu.fr/~lagree/COURS/CISM/RNSP_CISM.pdf`